Korea Maritime and Ocean University

The Graduate School

Department of Civil and Environmental Engineering

Crack Control and Performance Improvement for Pile to Concrete Pile-cap Connections of Integral Abutment Bridges

A Thesis in

Civil Engineering

by

Kyeongjin Kim

Advisor Jaeha Lee

Submitted in Partial Fulfillment
of the Requirements
for the Degree of

Master of Engineering

February 2015

본 논문을 김경진의 <u>공학석사</u> 학위논문으로 인준함.

위원장   경 갑 수   (인)

위 원   이 재 하   (인)

위 원   손 동 우   (인)

2015년 2월

한국해양대학교 대학원

TABLES OF CONTENTS

List of Tables

List of Figures

– ⅴ –

일체형 교대 교량 파일-교대연결부의 균열특성 및 구조성능 개선방안 연구

Crack Control and Performance Improvement for Pile to Concrete Pile-cap Connections of Integral Abutment Bridges

김 경 진

Department of Civil and Environment Engineering

Graduate School of Korea Maritime and Ocean University

초록

최근 늘어나는 교통량과 노후화로 인한 많은 문제를 발생시키고 있는 조인트 교량에 비해, 유지관리 비용이 저렴하고 시공이 간편한 일체형교대교량의 시공 사례가 늘어나고 있다. 북미와 유럽에서는 10,000개 이상의 일체형 교대교량이 사용중에 있으나(Arockiasamy et al. 2004) 국내에서는 시공 사례가 적을 뿐만 아니라, 이에 대한 연구도 미미한 실정이다. 일체형 교대 교량은 조인트를 제외 하고 교대와 상부구조물을 일체형으로 시공한 교량을 말한다. 기존의 조인트 교량은 신축이음장치의 차량 충격에 의한 파손과 이를 통한 누수 및 제설제의

침투로 교좌장치의 작동 불능, 잦은 파손으로 인한 교통 장애와 보수비용의 증가, 신축이음장치 및 교좌장치의 설계/시공으로 인한 시설비용의 증가, 상부구조와 하부구조의 연결부에서 지진하중, 풍하중에 대한 횡방향 저항성 취약 등의 문제점을 노출시켜 왔다. 그러나 일체형 교대교량은 신축이음장치의 제거를 통해 이러한 문제점을 개선할 수 있다. 하지만 이러한 일체형 교대 교량은 반복적인 온도하중에 따른 토질과 파일의 상호작용에 의해 파일-교대 연결부에 발생하는 균열이 문제점으로 지적되어 왔다. 미국과 유럽에서는 많은 연구가 진행되어 일체식 교대 교량의 거동 및 설계특성을 파악하고 이를 활용하여 설계를 시도하고 있으나 국내의 도로교설계기준 (2012)에서는 아직 일체식 교대 교량의 설계 지침에 관한 언급이 전무한 실정이며 1980년에 발간된 미국 FHWA Technical Advisory T 5140.13 (1980)의 추천사항에 대한 언급만 되어있다. 따라서 본 논문에서는 일체형 교대교량의 설계와 연구의 진행에 도움이 되고자, 일체형 교대 교량에서 발생 가능한 균열의 형상을 예측하고 균열 발생을 저감하기 위한 철근 상세 또는 연결부 상세를 제안하였다. 또한, 교대-파일 연결부 보강에 효과적인 것으로 확인된 나선 철근 형상의 변수연구를 통해 주요 변수를 확인하였다. 제안된 연결부는 크게 교대 자체의 강성을 높이는 방법과 강성을 줄이고 일정량의 변위를 허용하는 방법을 사용하였으며 강성을 높이는 방법에는 연결부에 나선 철근을 삽입하는 것이 효과적으로 확인되었으며 강성을 줄이고 일정량의 변위를 허용하는 방법에는 지중에 삽입되는 H 파일의 플랜지를 감소시키는 방법과, 변위를 허용하는 연결부가 일체식 교대교량의 균열 방지에 효과적인 것으로 나타났다. 또한 제안된 연결부는 교대로부터 전달되는 상부구조물의 반력을 감소시켜 상부구조의 내구성 및 구조건전성도 함께 향상시키는 것으로 확인되었다.

KEY WORDS: Integral abutment bridge 일체형 교대교량, Expansion joint 신축이음장치, Crack reducing 균열저감, Design 설계, Pile-to-pilecap connection detail 연결부 상세, Finite Element Method 유한요소해석법,

Chapter 1

Introduction

In this chapter, the integral abutment bridge is introduced, the differences between integral abutment bridges and conventional joints is given. The strong points and weak points of integral abutment bridges are shown. The objective of this study and research methodology is also given.

1.1 Problem Statement

Integral abutment bridges (IA bridges) have been successfully constructed and served in U.S. and Europe. The differences between IA bridges and conventional joint bridges (Conventional Joint bridges) are shown in Fig. 1-1. Integral abutment bridge reduce initial cost, maintenance cost and construction time due to removing expansion joints. Furthermore, IA bridges are expected to higher reliability and better vehicle driving by removing expansion joints. Bridges have expansion joints between the superstructure and columns to allow for expansion and contraction of the bridge to the temperature load. The expansion joints prevent additional stresses in the superstructure and columns due to temperature load. However, frequent maintenance cost and replacement cost is required due to intrusion of foreign substance of the running vehicle and the impact of vehicles (Fig. 1-2(a)). Also, It is expected to be increased in transportation costs due to traffic jam for repair and replacement of expansion joints. In terms of maintenance of the bridge, expansion joint destruction cause salt damage, leakage and malfunction of the shoe (Fig. 1-2(b)). Furthermore expansion joint buckled is caused car accident (Fig. 1-2(c)). When seismic load and excessive wind were occurred in bridge, it causes a lateral-displacement of the superstructure. IA bridges has complex behavior due to different boundary conditions and loads compared to CJ bridges. The superstructure and substructure does not influence each other's behavior due to expansion joints

and shoes. However, IA bridges influences lateral-loads of superstructure due to removing expansion joints and shoes.
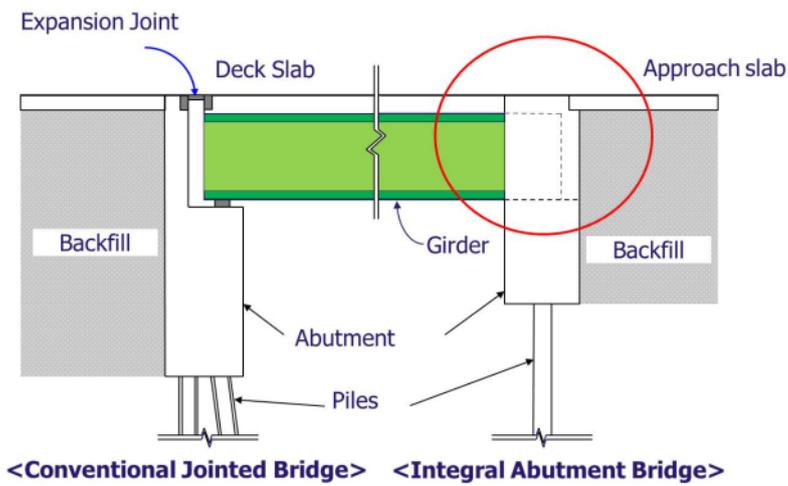
Fig. 1-1 Schematic of conventional jointed bridge and integral abutment bridge (Kim et al., 2013)

(b) Leakage & bearing deterioration

(a) Faulty joint   (c) Expansion joint buckled

(www.komonews.com, May 29, 2014)

Fig. 1-2 Expansion joint problems

Majority of the U.S. state agencies recommended the usage of IA bridges only for short or medium length bridges with weak-axis oriented steel HP piles and stub

abutment. This is primarily because the total length of IA bridge depends on the thermal expansion/contraction induced by temperature fluctuations and time-dependent effects.

In an integral abutment bridge, pile-to-pilecap performance is a important aspect. Since integral abutment bridges develop stresses due to daily and seasonal temperature changes (Fig. 1-3), pile-to-pilecap connections in IA bridges are vulnerable to thermal movement and seismic loading. The behavior and related response of IA bridges can not be easily predicted due to the complexity of soil-interaction, time-dependent effects, and temperature. Cracks may develop due to the above-mentioned complicated interactions with natural factors and can cause problems in the structure. Surprisingly, no specific detail on current bridge design code is available. Moreover, for integral abutment bridges it is necessary to consider time-dependent effects and horizontal load of the structure due to temperature load and soil-structure interaction. It can be mentioned that, previous studies only involved analyses regarding static increase/decrease in temperature and did not consider any hysteretic changes due to soil-structure interaction. Thus, this study intends to identify crack propagation patterns due to lateral loads and propose pile-to-pilecap connections for improved performance under lateral loadings.
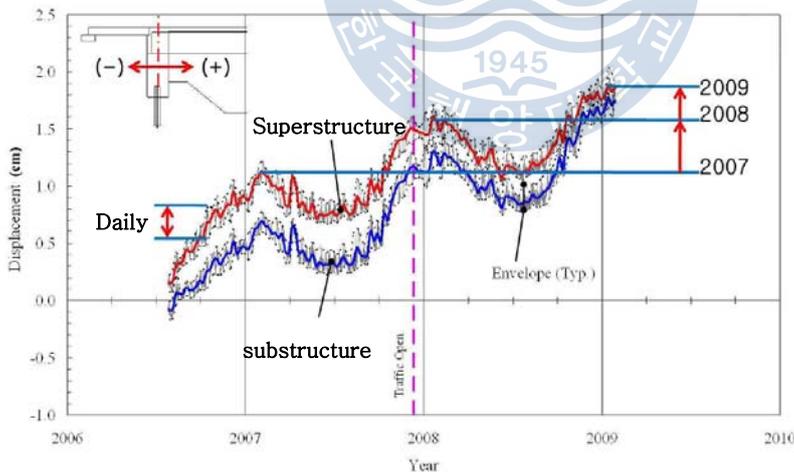
Fig. 1-3 Daily and seasonal temperature changes (Kim and Laman, 2010)

1.2 Objectives

Recently, IA bridge with increased length has been constructed. In U.S., 358 m long concrete girder IA bridge and 318 m long steel girder IA bridge have been successfully constructed and is currently in service, and much more IA bridges are expected to be constructed in future. The lengthening of IA bridge is depend on supporting pile performance since crack initiation and propagation are occurred around pile-to-pilecap connection due to a thermal movement. An increased length cause increased the effects of thermal loads. Accordingly, thermal movement of IA bridge become an issue due to the increased longitudinal displacement of superstructures (Lawver et al. 2007). Thus, pile-to-pilecap connection is one of the most important bridge components for length IA bridge. However, in Korea, design standard for integral abutment bridges is not specifies the connection details. So, the primary objective of this research is to improve the performance of pile-to-pile connection and crack control. In this study, 12 types of pile-to-pilecap connections are proposed for better performance under the increased thermal loads. The proposed types of pile-to-pilecap connection is evaluated for crack control and energy absorption. Furthermore, parametric studies of spiral rebar on pile-to-pilecap connection is conducted in this study.

A finite element model (FEM) was used to simulate the crack propagation in concrete, and the results of the numerical model was compared with the experimental data by Frosch et al. (2009).

1.3 Research Significance

According to Lawver et al. (2007), the temperature load has more influence on the bridge than the impact loading of vehicles. In order to expand the usability of a bridge for a long-term, research on integral abutment bridges has become crucial. However, as mentioned before, due to lack in specifications and details of IA bridge in Korea, reluctance is seen in such research. The rigid frame bridge, which

is similar to an IA bridge, has been used only in approximately 10 m length bridge. According to Korean transportation researches, if IA bridges are constructed instead of the existing CJ bridges, it is expected to reduce 540 billion initial cost and 60 billion maintenance cost every year. Therefore, the design guidelines is in need for IA bridges.

Due to the above-mentioned problems, the current study was conducted to improve integral abutment bridges, which have a number of advantages among the mid-short span bridges. Generally, the expansion joints in a long-span bridge are removed for improved performance and maintenance. Therefore, the results of this study are expected to be applied to the design and construction of long-span bridges.

1.4 Research Methodology

To accomplish the objectives of this study, the following tasks are established and flowchart of the research methodology is shown in Fig. 1-3.

- An introduction on integral abutment bridge and statement of problems of integral abutment bridge.

- Literature review is conducted.

- Numerical models are developed for evaluation.

- Numerical model is compared to Frosch's experimental data (2009) for verifications.

- To prevent crack propagation, increased stiffness method for pile-to-pilecap connections are proposed and evaluation of proposed connection type was conducted.

- To prevent crack propagation, flexible pile-to-pilecap connections are proposed, and evaluation of flexible pile-to-pilecap connection type is conducted.

• In order to evaluate proposed pile-to-pilecap connections, 3D finite element models were developed using Abaqus 12.1.

• Obtained 3D model data were used to predict the possible crack formations in the superstructure of the IA bridges.

• Among several different types of proposed model, pile-to-pilecap connections which showed better performance are selected.

```
┌─────────────────────────────────────┐
│           INTRODUCTION              │
│            Chapter  1               │
│  (1)  Problem  Statement,  Objectives │
└─────────────────────────────────────┘
                  │
                  ▼
┌─────────────────────────────────────┐
│         LITERATURE  REVIEW          │
│            Chapter  2               │
│  (1)  Conducted  Researches  Review  │
│        (2)  Numerical  Model         │
└─────────────────────────────────────┘
                  │
                  ▼
┌─────────────────────────────────────┐
│      THEORETICAL  BACKGROUND        │
│            Chapter  3               │
│      (1)  Material  for  Concrete    │
│       (2)  Material  for  Steel      │
│           (3)  Contact              │
└─────────────────────────────────────┘
                  │
                  ▼
┌─────────────────────────────────────────────────┐
│              NUMERICAL  MODEL                    │
│                Chapter  4                        │
│      │                           │              │
│      ▼                           ▼              │
│  ┌──────────────────────┐   ┌─────────────────┐ │
│  │(1) Numerical model   │   │(3) Pile-to-pilecap│
│  │    development       │   │    connection    │ │
│  └──────────────────────┘   │     propose      │ │
│      │                      └─────────────────┘ │
│      ▼                           │              │
│  ┌──────────────────────┐        │              │
│  │(2) Numerical model   │        │              │
│  │    verification      │        │              │
│  └──────────────────────┘        │              │
│      │                           │              │
│      ▼                           ▼              │
│  ┌─────────────────────────────────────────┐    │
│  │(4) Proposed pile-to-pilecap connection   │   │
│  │    analysis                             │    │
│  └─────────────────────────────────────────┘    │
│                  │                              │
│                  ▼                              │
│         ┌─────────────────┐                     │
│         │ (5)  Evaluation │                     │
│         └─────────────────┘                     │
└─────────────────────────────────────────────────┘
                  │
                  ▼
┌─────────────────────────────────────┐
│  CONCLUSION  AND  RECOMMENDATIONS   │
│            Chapter  5               │
└─────────────────────────────────────┘
```
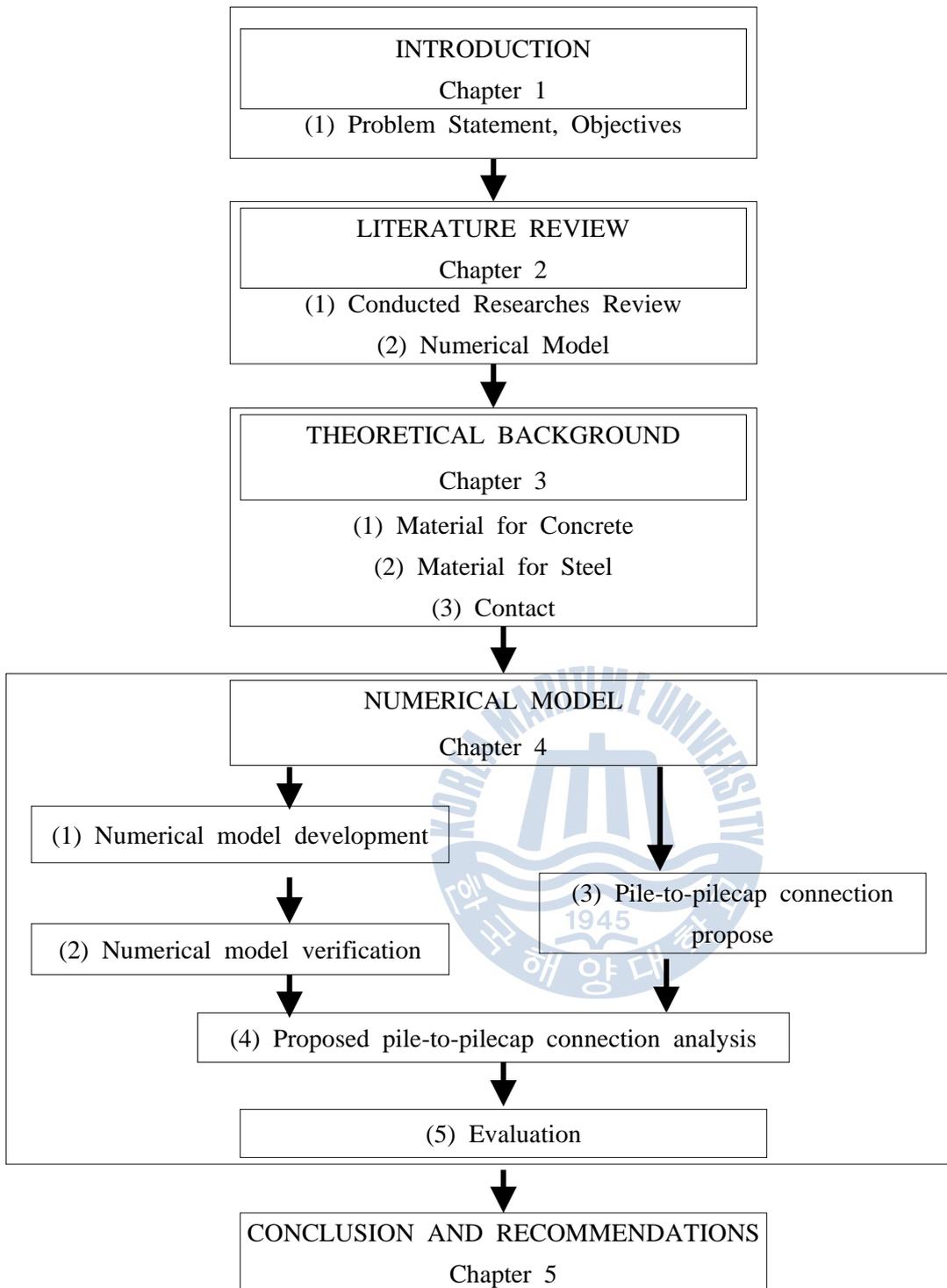
Fig. 1-4 Thesis flow chart

Chapter 2

Literature Review

This chapter reviews the past researches conducted in the area of integral abutment bridges. Especially, the research to cover the weak points of integral abutment bridge is focused and reviewed. Furthermore, section regarding Numerical model is described. A summary of the literature review is also given at the end of this chapter.

2.1 Research about IA bridges

This section reviews the past conducted researches about structural performance of integral abutment and effects of thermal load in integral abutment.

2.1.1 Research about Structural Performance of Integral Abutment Bridges

After conducting a 75-year cyclic load testing for concrete pile, steel pipe pile and weak-axis oriented supporting pile, Arsoy et al. (2002) found that the weak-axis oriented supporting pile was a reasonable choice for IA bridge. This is because ductility and less stiffness of IA bridge matched closely. Ductile and low stiff pile-to-pilecap connection can prevent cracks in the pilecap. Therefore, this is important to increase the IA bridge length, reduce the axial force in the superstructure and allow larger displacement without generating any concrete crack.

In the research of Frosch et al. (2009), four tasks were performed. Development of a series of designs of ground motions representing current estimates of the seismic hazard in Indiana, experimental test of current and proposed details of the pile-to-pilecap connection to estimate displacement capacity, evaluation of field data collected during an existing long-term integral abutment bridge monitoring project to estimate the relationship between abutment movements and earth pressures, and construction of numerical models to estimate seismic displacements of the abutment.

Specific results can be found in Frosch et al. (2009).

Ahn et al. (2011) examined the abutment-pile connection in the integral abutment bridge to improve the shear and bearing resistance of pile-to-pilecap connection. Loading tests and FE analysis of half scale pile-to-pilecap connection specimens were performed to evaluated the stiffness and behaviors of the proposed details. The results indicated that the proposed pile-to-pilecap connections were efficient due to sufficient stiffness, rotational stiffness and bearing strength.

Results of long-term monitoring studies of integral abutment bridges by Kim and Laman (2012) showed that, unrecoverable residual displacement increased every year consistently. Axial-load and moment was present in the superstructure, which can cause moment and moment of inertia due to the shift displacement in substructure. Moreover, the stiffness of pile near the support pile changed frequently due to temperature load and interaction of soil-structure. The displacement of abutments due to this frequent temperature load causes fatigue loads on the support piles that were installed in a line. Therefore, it is difficult to predict the behavior of the bridges due to time-dependent effects, boundary conditions of soil, annual temperature and daily temperature fluctuations.

2.1.2 Research about Thermal Loads in Integral Abutment Bridges

In the research of Dicleli and Albhaisi (2003), analytical equations are developed to estimate the effects of cyclic thermal loading on the performance of H-piles in integral abutment bridges with stub-abutments. The cyclic displacement capacity of steel H-piles decreases as the foundation soil becomes stiffer, the effect of the orientation of the steel H-piles on the displacement capacity is negligible. A pinned abutment-pile connection increases the displacement capacity of integral bridges under cyclic loading. Concrete bridges are less sensitive to temperature variations, therefore, concrete bridges are more suited for integral bridge construction.

Kim and Laman (2010) developed a numerical modeling methodology for long-term simulation and demonstrated characterization methods for the key parameters of integral abutment bridges. The magnitude of the thermal expansion

– 9 –

coefficient and the length of the bridge significantly influenced the girder axial force, pile lateral force, pile moment and pile head displacement. At mid-span, the influence of the bridge length was weak on the girder positive moment. The influences of backfill height and stiffness parameters were insignificant. The increased soil stiffness increased the girder moment, pile lateral force and pile moment, but reduced the pile head displacement.

Kalayci et al. (2012) conducted the parametric FE study on the effect of curvature on the seasonal response of two span curved IA bridges. Increased the curvature, longitudinal displacements, earth pressures and weak axis bending moment on pile were decreased. As the curvature increased, the lateral displacements increased. The superstructure displacements at the bridge ends were only affected by backfill soil type. The bending stresses on the bridge superstructure was decreased compared to the straight IA bridge.
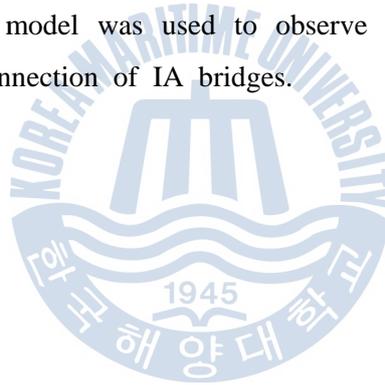
2.2 numerical Model

Lee et al. (1998) proposed the material model for concrete (Concrete damaged plasticity), According to Abaqus manual, the concrete damaged plasticity model is a solid material model to provide a picture of the behavior of concrete elements for the analysis of concrete structures under cyclic or dynamic loading. When a pressure is applied, the main failure mechanisms that originates are cracking due to tension and crushing due to compression. The main purpose of the concrete damaged plasticity theory is to capture the effects of irreversible damage associated with the failure mechanisms. These effects follow different yield strengths in compression and tension. The effects follow softening behavior under tension. however the initial hardening following softening behavior in compression, stiffness recovery effects during cyclic loading and rate sensitivity, especially the peak strength with strain rate is increased. Specific information regarding material models will be explained in later section.

2.3 Summary of Literature Review

Based of the literature review conducted, important knowledge is summarized below. This information was used for planning the evaluation.

- The weak-axis oriented steel pile is a proper choice for IA bridges due to reasonable stiffness and ductility. Development of pile-to-pilecap connection with low stiffness and ductility is the key to increase the length of IA bridges without failure of the pile-to-pilecap connection.

- Unrecoverable residual displacement of IA bridges increased every year consistently.

- Concrete bridges are more suited for the integral abutment bridge construction due to less sensitive to temperature variations.

- The magnitude of the thermal expansion coefficient influenced the girder axial force, pile lateral force, pile moment and pile head displacement.

- Concrete damaged plasticity model was used to observe the performance of concrete in pile-to-pilecap connection of IA bridges.

Chapter 3
Theoretical Background

This chapter describes the material model and material properties for numerical analysis. The concrete material model is important in this study in order to predict the crack initiation as well as propagation around pile-to-pilecap. Furthermore, possible contact option between H-pile and pilecap is described.

3.1 Material Model for Concrete

Selected concrete model is concrete damaged plasticity model which was originally developed by Lubliner et al. (1989) and further developed by Lee and Fenves (1998). Specific information regarding the concrete damaged plasticity model can be found in Abaqus manual as shown below.

- The concrete damaged plasticity model provides a general capability for modeling concrete and other quasi-brittle materials.

- To represent the inelastic behavior of concrete, the concrete damaged plasticity model uses isotropic damaged elasticity in combination with isotropic tensile and compressive plasticity.

- The concrete damaged plasticity model can be used for plain concrete, even though it is intended primarily for the analysis of reinforced concrete structures

- Steel rebar can be used with the concrete damaged plasticity model for analysis.

- Concrete damaged plasticity model is designed for the behavior of various loading under low confining pressures such as monotonic, cyclic, and dynamic loading.

- The concrete damaged plasticity consists of the combination of nonassociated

multi-hardening plasticity and scalar (isotropic) damaged elasticity to describe the irreversible damage that occurs during the fracturing process.

- The concrete damaged plasticity can control of stiffness recovery effects during cyclic load reversals.

- The concrete damaged plasticity can be sensitive to the rate of straining.

- The concrete damaged elasticity can be used in conjunction with a viscoplastic regularization in Abaqus/Standard to improve the convergence rate in the softening regime.

- The elastic behavior of the material should be linear and istropic.

The stress-strain relations are given by scalar damaged elasticity

$$\sigma = (1-d)D_0^{el} \cdot (\epsilon - \epsilon^{pl}) \tag{1}$$

D_0^{el} : initial (undamaged) elastic stiffness of the material

d : scalar stiffness degradation variable (0<d<1)

Fig. 3-1 and Fig. 3-2 shows the response of concrete to uniaxial loading in tension and compression. According to Abaqus, under uniaxial tension, the stress-strain curve is increased linearly until the σ_{t0}. The failure stress is decreased non-linearly to the onset of micro-cracking in the concrete material. In plastic region, after σ_{t0}, the response is typically characterized by stress hardening followed by strain softening beyond the σ_{cu}. Under uniaxial compression the stress-strain response follows a linear until initial yield. The response in plastic region is generally characterized by stress hardening followed by strain softening beyond the ultimate stress. The tension-softening relation is following CEB-FIP 2010 (Fig. 3-3 and Fig. 3-4). Under uniaxial tension the stress-strain response follows a linear elastic until failure stress (Fig. 3-1). At 90% of the tensile strength f_{ck}, micro-cracking starts to reduce the stiffness. The formula is given

$$\sigma_{ct} = E_{ci} \cdot \epsilon_{ct} (\sigma_{ct} \leq 0.9 \cdot f_{ctm}) \tag{2}$$

$$\sigma_{ct} = f_{ctm} \cdot (1 - 0.1 \cdot \frac{0.00015 - \epsilon_{ct}}{0.00015 - 0.9 \cdot f_{ctm}/E_{ci}})(0.9 \cdot f_{ctm} < \sigma_{ct} \leq f_{ctm}) \qquad (3)$$

E_{ci} : tangent modulus of elasticity in (MPa)

ϵ_{ct} : tensile strain

σ_{ct} : tensile stress in (MPa)
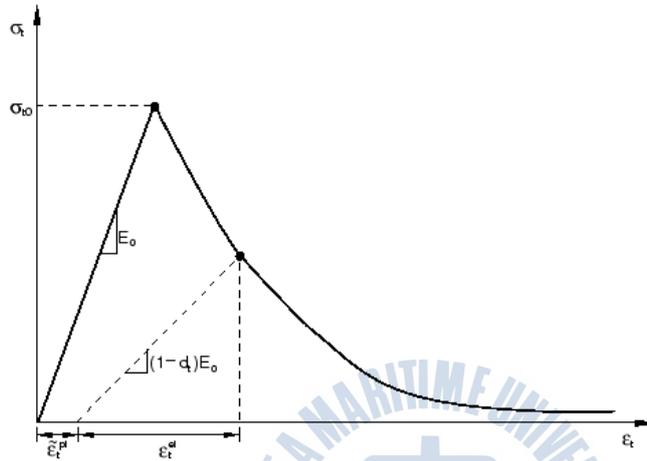
f_{ctm} : tensile strength in (MPa)

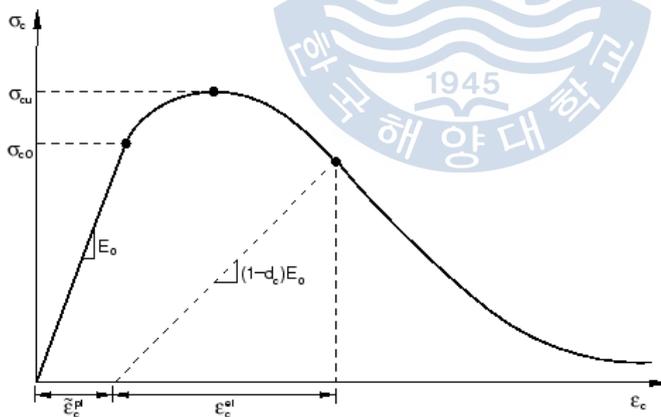Fig. 3-1 Response of concrete to uniaxial loading in tension

Fig. 3-2 Response of concrete to uniaxial loading in compression

- 14 -

This micro-cracking is increased close to the tensile strength. All stresses and deformations in the fracture process zone can be related to a fictitious crack opening w (Fig. 3-4).

$$f_{ctm} = 0.3 \bullet (f_{ck})^{2/3} \quad \text{concrete grades} \leq C50 \tag{4}$$

$$f_{ctm} = 2.12 \bullet \ln(1 + 0.1 \bullet (f_{ck} + \triangle f)) \quad \text{concrete grades} > C50 \tag{5}$$
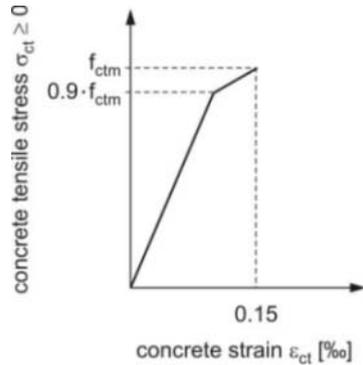
$$G_F = 73 \bullet f_{cm}^{0.18} \tag{6}$$

Fig. 3-3 Schematic representation of
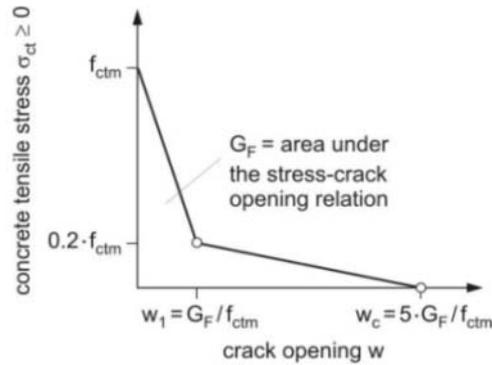the stress-strain for uniaxial tension

Fig. 3-4 Stress-crack opening relation
for uniaxial tension

Fig. 3-5 shows a uniaxial load cycle assuming the default values for the stiffness recovery factors. The tensile stiffness is not recovered as the load changes from compression to tension once crushing micro-cracks have developed. This behavior is the default used by Abaqus.

The yield surface in plastic strain is shown in Fig. 3-6. The concrete damaged plasticity model uses a yield condition based on the yield function proposed by Lubliner et al. (1989) and incorporates the modifications proposed by Lee and Fenves (1998) to account for different evolution of strength under tension and compression.
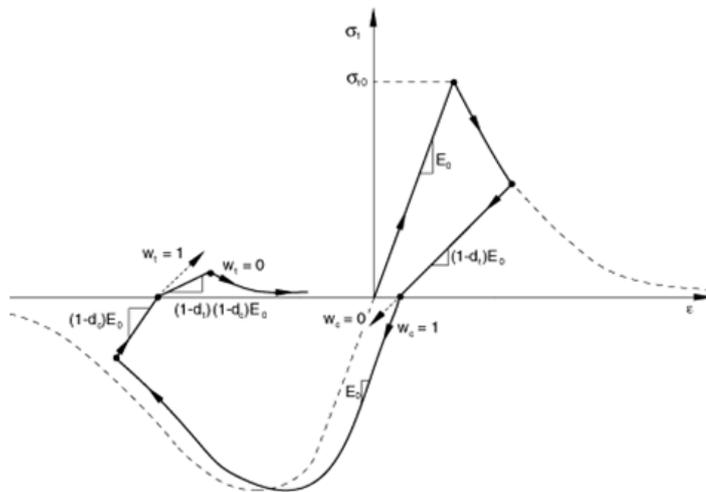
Fig. 3-5 Uniaxial load cycle curve (tension-compression-tension)
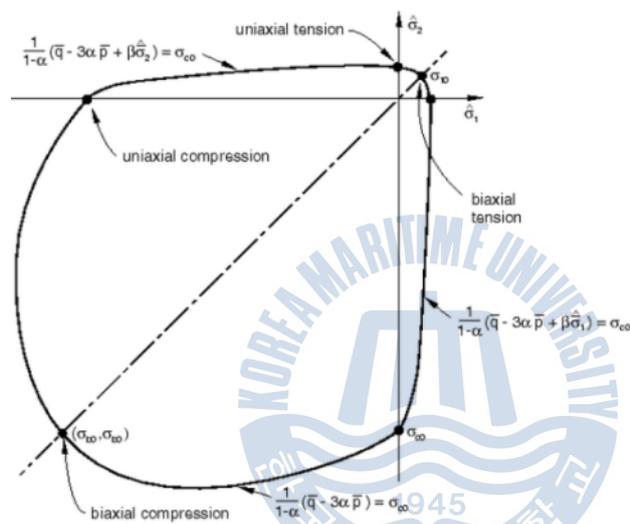
Fig. 3-6 Yield surface in plane stress

3.2 Material Model for Steel Rebar and H-pile

Elasto-plastic model was used for steel material. Elastic behavior is recoverable behavior. If the load exceeds some limit, the deformation is no longer fully recoverable, some parts of the deformation is not recoverable after load is removed, Specific information regarding the elastic model is shown below.

· Elastic material model is valid for small elastic strains (normally less than

- 16 -

5%).

- Elastic material model can be isotropic, orthotropic, or fully anisotropic.

- Elastic material model can have properties that depend on field variables.

- Elastic material model can be defined with a distribution for solid continuum elements in Abaqus/Standard.

The total stress is defined as shown below equation.

$$\sigma = D^{el}\epsilon^{el} \tag{7}$$

σ : Total stress

D^{el} : The fourth-order elasticity tensor

ϵ^{el} : The total elastic strain

The simplest form of linear elasticity is the isotropic case, and the stress-strain relationship is given by

$$\begin{bmatrix} \epsilon_{11} \\ \epsilon_{22} \\ \epsilon_{33} \\ \gamma_{12} \\ \gamma_{13} \\ \gamma_{23} \end{bmatrix} = \begin{bmatrix} 1/E & -\nu/E & -\nu/E & 0 & 0 & 0 \\ -\nu/E & 1/E & -\nu/E & 0 & 0 & 0 \\ -\nu/E & -\nu/E & 1/E & 0 & 0 & 0 \\ 0 & 0 & 0 & 1/G & 0 & 0 \\ 0 & 0 & 0 & 0 & 1/G & 0 \\ 0 & 0 & 0 & 0 & 0 & 1/G \end{bmatrix} \begin{bmatrix} \sigma_{11} \\ \sigma_{22} \\ \sigma_{33} \\ \sigma_{12} \\ \sigma_{13} \\ \sigma_{23} \end{bmatrix} \tag{8}$$

E : Young's modulus

ν : Poisson's ratio

G : The shear modulus

In Abaqus/Standard spatially varying isotropic elastic behavior can be defined for homogeneous solid continuum elements by using a distribution. The distribution must include default values for E and ν. If a distribution is used, no dependencies on temperature and/or field variables for the elastic constants can be defined.

Plasticity theories model the material's mechanical response as it undergoes such nonrecoverable deformation in a ductile fashion. The plasticity model was applied

to soils, concrete, rock, ice, crushable foam, and so on. Most of the plasticity models in Abaqus are incremental theories in which the mechanical strain rate is decomposed into an elastic part and a plastic part.

- A yield surface, which generalizes the concept of yield load into a test function that can be used to determine if the material responds purely elastically at a particular state of stress, temperature, etc.

- A flow rule, which defines the inelastic deformation that occurs if the material point is no longer responding purely elastically.

- Evolution laws that define the hardening-the way in which the yield and/or flow definitions change as inelastic deformation occurs.

Furthermore, Abaqus/Standard has a deformation plasticity model, in which the stress is defined from the total mechanical strain. This is a Ramberg-Osgood model and is intended primarily for ductile fracture mechanics applications, where fully plastic solutions are often required.

3.3 Contact

The contact option between abutment and H-pile was general contact in this research. According to Abaqus 6.13 manual, contact interactions in a model can refer to a contact property definition, it is almost same way that elements refer to an element property definition. By default, the surfaces interact only in the normal direction to resist penetration. The other mechanical contact interaction models available depend on the contact algorithm and whether Abaqus/Explicit 6.13 is used. The contact options were softened contact and hard contact. Three types (a linear law (Fig. 3-7), a tabular piecewise-linear law (Fig. 3-8), and an exponential law (Fig. 3-9)) of softened contact are available in Abaqus. In Abaqus, the softened contact relationships are specified in terms of overclosure versus contact pressure for contact involving element-based surfaces and for element based contact.

To contact involve a node-based surface or nodal contact elements for which an area or length dimension is not defined, softened contact is specified in terms of overclosure (or clearance) versus contact force. In Abaqus/Explicit 6.13, If the general contact algorithm is being used for slave surfaces on beam-type elements, specify pressure as force per unit area. The softened contact option might be used to model a soft, thin layer on one or both surfaces. In Abaqus/Standard, The softened contact options are also sometimes useful for numerical reasons because they can make it easier to resolve the contact condition.
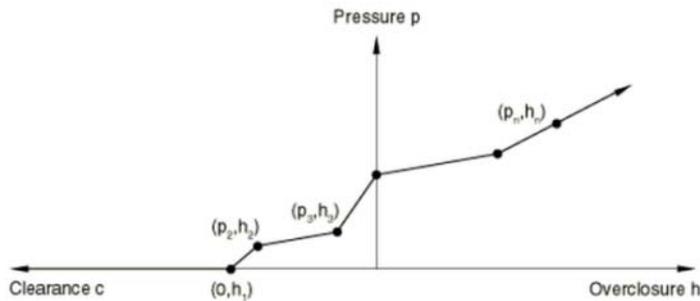

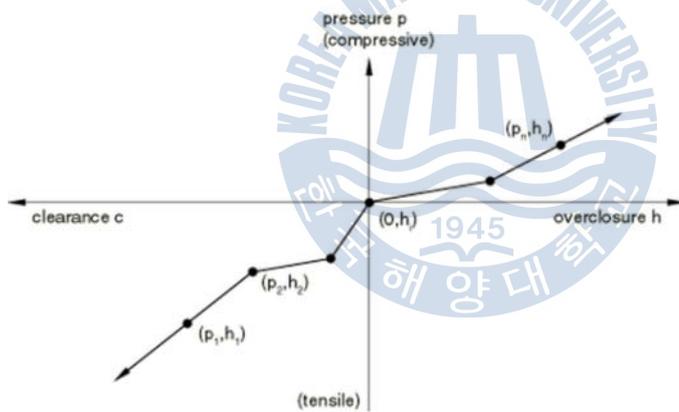Fig. 3-7 "Softened" pressure-overclosure relationship defined in tabular form

Fig. 3-8 Piecewise linear "softened" pressure-overclosure relationship with tensile behavior in Abaqus/Explicit
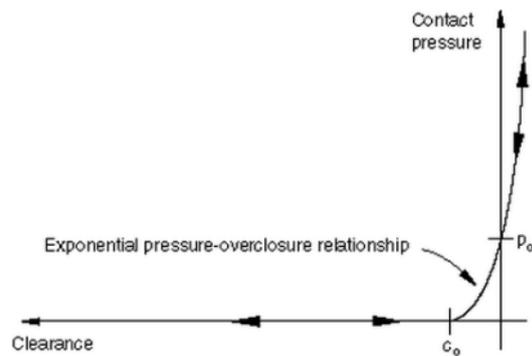
Fig. 3-9 Exponential "softened" pressure-overclosure relationship in
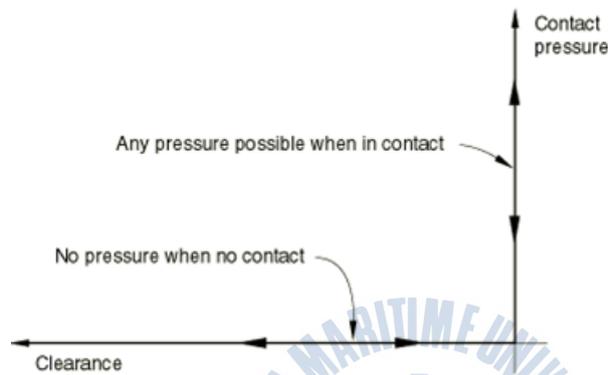Abaqus/Explicit

Fig. 3-10 Default pressure-overclosure relationship of "hard"contact

In this study, the hard contact was used. The hard contact relationship minimizes the penetration of the slave surface into the master surface at the constraint locations and does not allow the transfer of tensile stress across the interface. A hard contact pressure-overclosure relationship is used for both surface-based contact and element-based contact. The hard contact include a nondefault contact pressure-overclosure relationship in a specific contact property definition. The common contact pressure-overclosure relationship is shown in Fig. 3-10, the zero-penetration condition can be enforced or can not be enforced depending on the constraint enforcement method used. Surfaces are in contact, Any contact pressure can be transmitted between them. The surfaces can be separated when the contact pressure reduces to zero, separated surfaces come into contact when the

clearance reduces to zero. Force is transmitted between nodes only zero distance, however in softened contact, in between the defined initial clearance, a larger number of nodes can be found for transmission. In this study, initial clearance is zero between HP pile and pilecap, therefore, the hard contact is the best choice.

Chapter 4

Numerical Analysis

This chapter describes a numerical model to analyze and observe the behavior of proposed pile-to-pilecap connection. Model verification is conducted in this chapter, and boundary conditions are considered to observe the performance.

4.1 Numerical Model Development

In this section, the numerical model for analysis is described. The pile size, pilecap size, spring model and boundary conditions are described.

4.1.1 Description of Numerical Model

The numerical model is shown in Fig. 4-1. A real scale experimental study conducted by Frosch et al. (2009) was selected in order to verify developed models using Abaqus 6.13. Material properties were obtained from the same experimental study. Elastic modulus of concrete was 21.76 GPa, fracture energy of concrete was 126 N/m, compressive strength and tensile strength of the concrete were 20.68 MPa and 2.26 MPa. the poisson's ratio for the concrete was 0.2, the density of the concrete was 2400 kg/m^3, Elastic modulus for the steel was 200 GPa, the yield strength of the steel was 522 MPa, the poisson's ratio for the steel was 0.32 and the density of the steel was 7400 kg/m^3. Embedded depth was 450 mm for this study. The concrete pilecap was assumed as a stub-type abutment which is a typical type. The model used 3D nonlinear solid elements for the pilecap and H-pile, And steel rebar was used 3D beam element. For contact condition between the pilecap and pile, 'hard' contact was used. "hard" contact does not allow the penetration of the slave surface into master surface. At the top of the pilecap, there is a rotational spring which is superstructure because when there is behavior of lateral displacements, rotational capacity influences rotation behavior. In this study, the soft ground condition is not considered. The soft ground condition is expected

dCollection

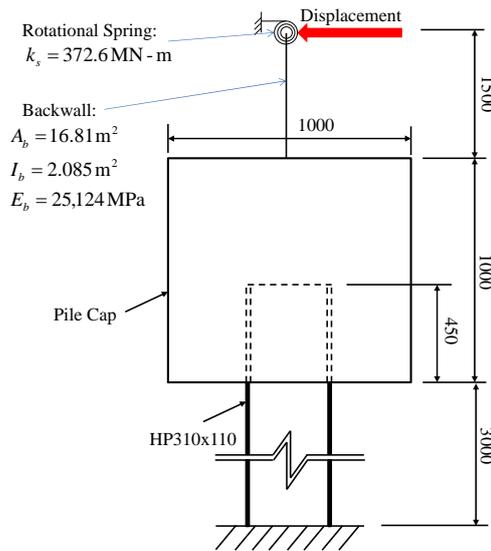to show the different behavior due to passive earth pressure.

Fig 4-1 Schematic of numerical model setup

4.1.2 Numerical Model Setup

A Simplified model setup was presented in Fig. 4-1. The concrete pilecap was 1 by 1 by 1 m^3 square solid element and the abutment is stub-type abutment. Pilecap and single supporting weak-axis oriented H-pile were considered in the numerical models. Backwall was simplified using beam elements to reduce the complexity of the model. Differential rotation between superstructure and substructure reported by Kim and Laman (2012) was also considered using rotational stiffness (κ_s) based on a typical four prestressed concrete girder superstructure. This study also utilized equivalent cantilever pile length (3 m) to exclude nonlinear soil strata boundaries in model according to Frosch et al. (2009). A 100 mm lateral displacement was applied to observe the crack patterns. In previous study, it was found that lateral displacement in pilecap is gradually increasing due to accumulated and unrecoverable residual displacement every year (Kim and Laman, 2010). Therefore, large deformation such as 100 mm of lateral displacement at pilecap was considered for this study.

4.1.3 Verification of Numerical Model

The analysis results of numerical model is shown in Fig. 4-2. The results of experimental data and numerical model are matched each other. It should be noted that displacement is estimated based on elastic deformations of the clamping rods due to the applied load as described in Frosch et al. (2009). The crack initiation and propagation were occurred around pile. The strain-stress data of elements was removed from the actual behavior of the pile-to-pilecap connection. Therefore, the numerical result data is not presented in Fig. 4-2 after crack propagation. The maximum forces of experiment was 111 kN. And numerical model was 106 kN. The difference in load between experiment data and numerical model was within 4%, and the difference in displacement between experiment data and numerical model was within 12% at maximum loads. In experiment, structural frame test can make gap between the supports and a loading point. Therefore, 12% difference can be acceptable for model verification.
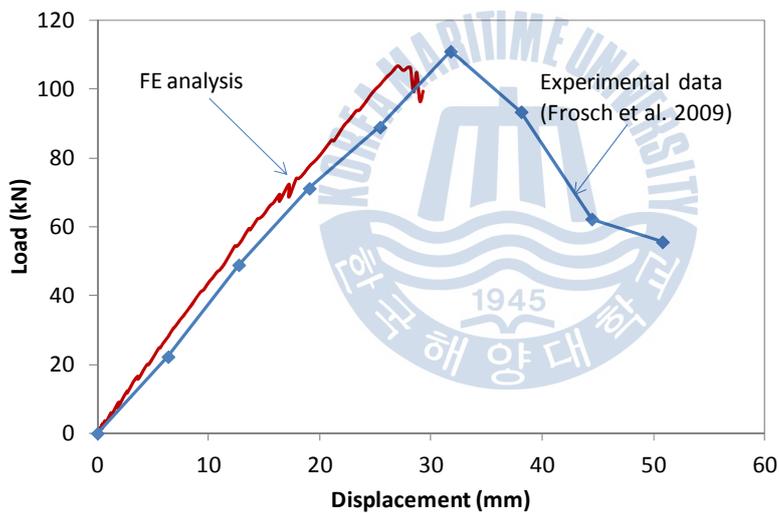

Fig. 4-2 Comparison of numerical model and experimental data

Crack patterns are shown in Fig. 4-3. FEM crack patterns were very similar to the experimental crack patterns. The cyclic loads were applied in experimental conditions, however one directional displacement was applied in numerical model. Therefore, numerical model showed a crack which is one direction. Based on a

results of numerical model, the model material and modeling methods could be reliable for study of pile-to-pilecap connections.
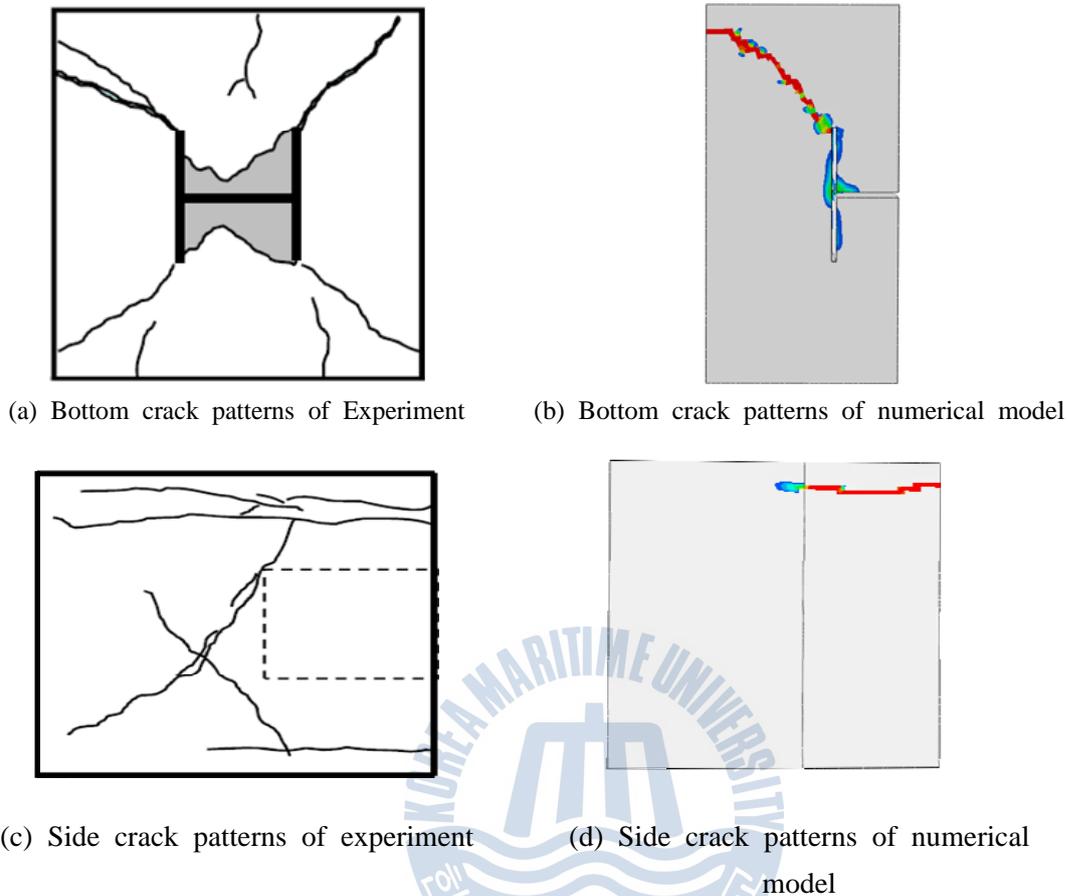

(a) Bottom crack patterns of Experiment   (b) Bottom crack patterns of numerical model

(c) Side crack patterns of experiment   (d) Side crack patterns of numerical model

Fig. 4-3 Crack patterns of experiment and numerical model

4.2 Performance in Various Boundary Conditions

In this section, before pile-to-pilecap connection analysis, considered various boundary conditions are described. Embedded length of H-pile, rotation and lateral translation is considered to observe the performance of the pilecap.

4.2.1 Structural Performance depending on Embedded Length

The performance of the pilecap was evaluated with embedded length, It is a important parameter to determine moment capacity of the concrete pilecap. Selected

Collection

embedded length is 300 mm, 450 mm and 600 mm. Fig. 4-4 show detail of embedded depth, Fig. 4-5 shows load-displacement graph depend on each embedded depth. It was found that increased embedded depth can increase the resistant capacity of pilecap. And it was increased linearly. Therefore, increased embedded depth can improve the resistant capacity of the pile-to-pilecap connection.
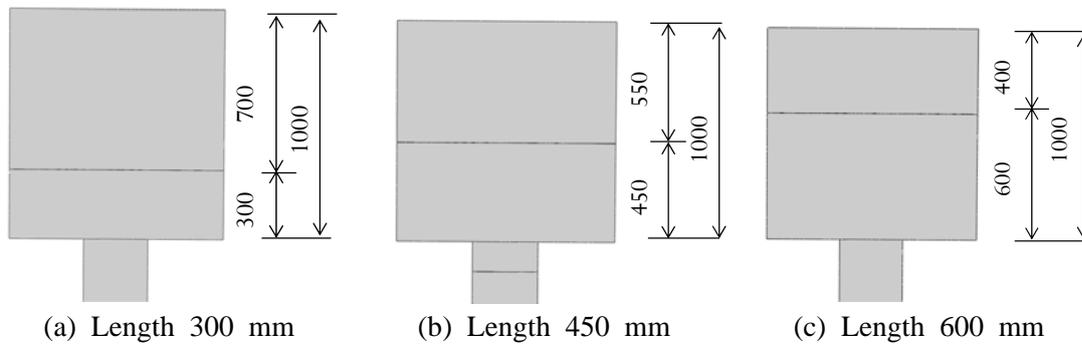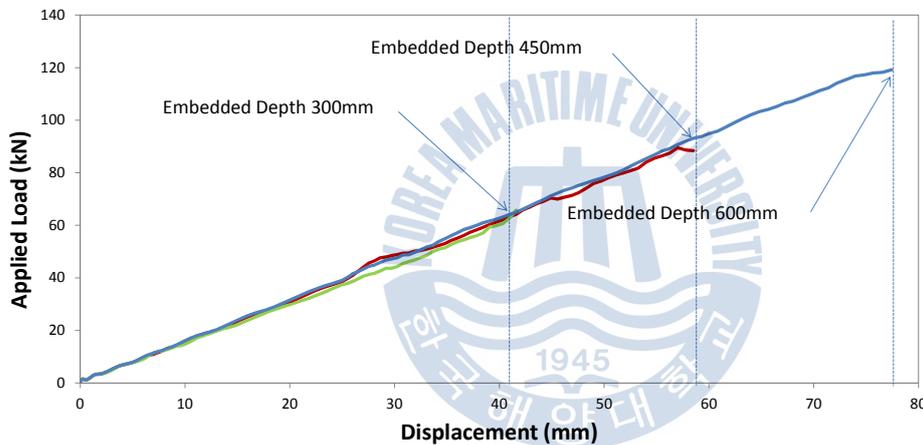

(a) Length 300 mm   (b) Length 450 mm   (c) Length 600 mm

Fig. 4-4 Detail of embedded depth

Fig. 4-5 Effect of embedded depth on load-displacement graph

4.2.2 Behavior of IA Bridge according to Various Boundary Conditions

In this study, three boundary conditions were considered. One was TO (Translation Only) model (Fig. 4-6(b)), another was RO (Rotation Only) model (Fig. 4-6(c)), and the other was RO + TO (Rotation only + Translation only) model (Fig. 4-6(d)). Each boundary conditions are shown in Fig. 4-6. In most integral abutment bridges, pilecap is designed as a stub-type, pile-to-pilecap

connection allows laterally movement more than rotation movement. It does not allow much of rotation. On the other hand, If a higher pilecap is used, the pile-to-pilecap connection is likely to rotate, however it does not allow much of laterally translation. Therefore, translation and rotation were considered as 'TO model' and 'RO model' to investigate the crack patterns upon pilecap behavior. In real behavior of IA bridge, rotation and translation are occurred at the same time. Therefore, the RO + TO model was used as standard model for proposed developed pile-to-pilecap connection.

(a) Conventional Model   (b) TO model
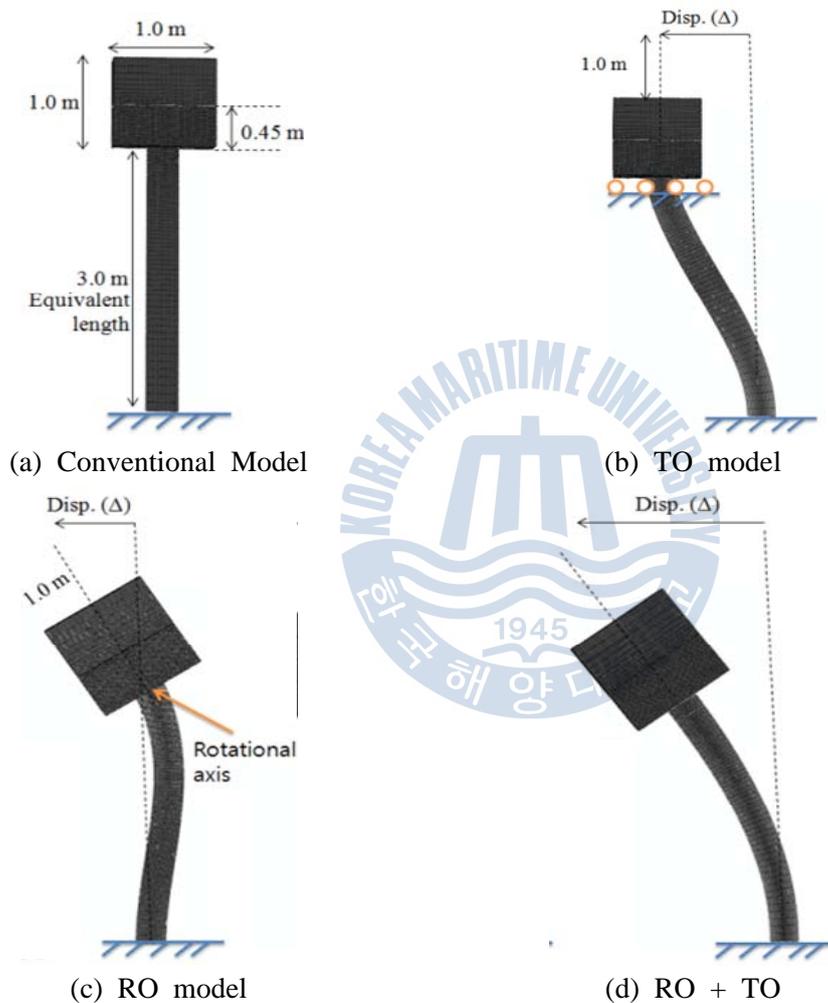
(c) RO model   (d) RO + TO
Fig. 4-6 Effect of boundary conditions on shape of deformation

The crack patterns are shown in Fig. 4-7. Arrows are direction of displacement

load. Crack were initiated from bottom surface of the pilecap near the H-pile. The crack directions of TO model and RO model were opposite to each other. The crack direction of TO model was same with loading direction, however the crack of RO model occurred opposite direction to the load direction. The crack was occurred from the edge of H-pile flange due to a contact force. The RO + TO model showed better performance and delayed crack initiation than other two cases since simultaneous translational and rotational movement compensate each of the influences. RO + TO model was expected to exhibit four-way diagonal crack propagation, but the results showed that similar results to TO because all models used a stub-type, 1 m-high pilecap. Depending on the bridge abutment geometries and boundary conditions, i.e., abutment height, soil stiffness, etc., a TO or RO crack pattern may occur in actual bridges.
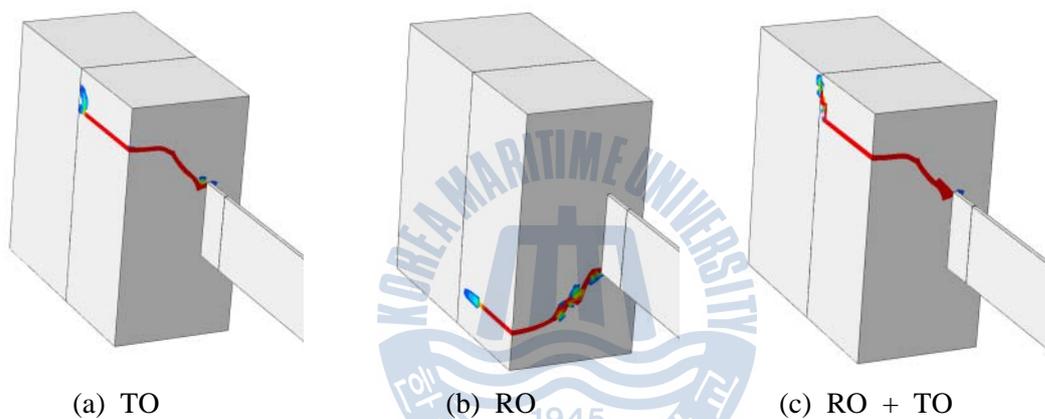
(a) TO   (b) RO   (c) RO + TO
Fig. 4-7 Crack patterns in pilecap depending on boundary condition

Load-displacement graph of three boundary conditions is shown in Fig. 4-8. The stiffness was increased linearly. The RO + TO model shows better performance than TO model and RO model. When same applied force was given, the RO + TO model has more energy absorption.
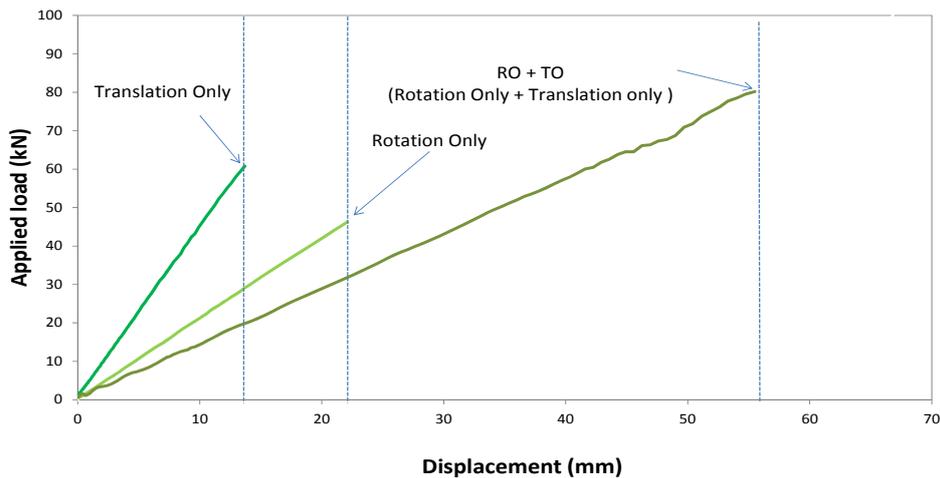
Fig. 4-8 Load-displacement graph depending on boundary conditions

## 4.3 Proposed Pile-to-pilecap Connection

In this section, proposed pile-to-pilecap connection and the results of the analysis is described. Load-displacement curves is given at the end of this section.

4.3.1 Proposed Pile-to-pilecap Increased Stiffness Connection Type.

The PennDOT connection type and the spiral rebar connection type are shown in Fig. 4-9. Currently, bridge design specifications stipulate the rebar details for connection. The PennDOT connection type was made by Pennsylvania University (2007). PennDOT DM-4 specifies the rebar detail, however it was developed to prevent from down-drag force in the supporting piles. A 900 mm length D19 rebar is embedded in the pilecap with H-pile in this model. In spiral rebar connection type, spiral rebar is embedded around pile in pilecap. It is easy to install and effective for seismic loads according to Frosch et al. (2009) and Kim et al. (2013). Both connection types are expected to prevent from crack propagation due to the increased stiffness. And parametric study of spiral rebar is given at the end of this chapter. Obtained results from PennDOT and spiral details can be found in Kim et al. (2013).
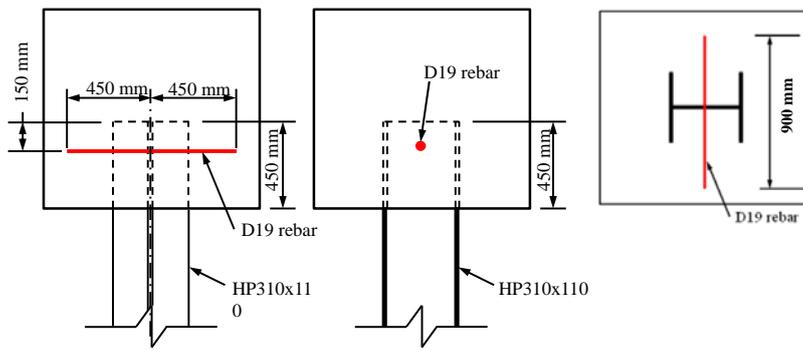
(a) PennDOT connection type
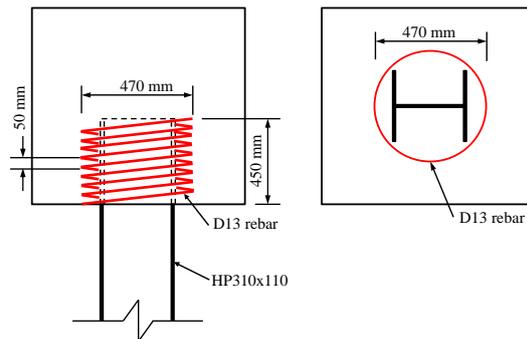
(b) Spiral rebar connection type
Fig. 4-9 Detail of PennDOT and spiral rebar connection type

The HSS tube connection type and square rebar connection type are shown in Fig. 4-10. Both connection types are similar to the spiral rebar connection type. The HSS tube connection type is embedded in pilecap. Also, this connection type is easy to install. And it is expected that the steel tube could prevent from crack propagation due to the increased stiffness at the bottom of the pilecap. In square rebar connection type, D13 rebar is embedded in pilecap in place of spiral rebar. This connection type is expected to reduce crack propagation due to the increased stiffness. And the parametric study of this model is presented at the end of this chapter.

- 30 -

(a) HSS tube connection type   (b) Square rebar connection type
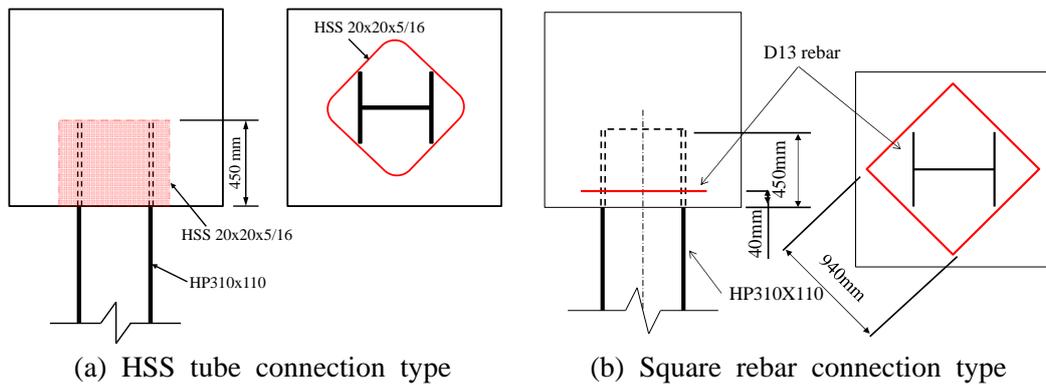
Fig. 4-10 Detail of HSS tube connection type and square rebar connection type

The grid rebar connection type is shown in Fig. 4-11. Four D29 steel rebars are embedded in the pilecap like grid near the H-pile. This connection type is expected to reduce the crack propagation due to increased stiffness.
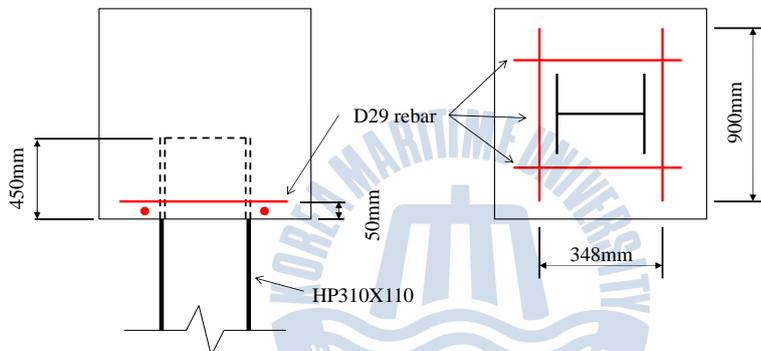

Fig. 4-11 Detail of grid rebar connection type

4.3.2 Proposed Pile-to-pilecap Flexible Connection Types

The removed flange connection type and the reduced flange connection type are shown in Fig. 4-12. Both connection types are expected to increase flexible behavior. Furthermore, removed flange connection type is expected to reduce stress concentration since previous study have shown that the crack was initiated from the H-pile flange. In removed flange connection type, two steel plates is welded on the bottom of the pilecap to resist the transferred axial force from the superstructure effectively. And D19 rebar is embedded in pilecap to protect from down-drag force

- 31 -

in the supporting piles. The stiffness of the pile-to-pilecap connection is expected to be minimized and mitigated. The reduced flange connection type is shown in Fig. 4-12(b). The flange of the H-pile was reduced under the pilecap. The reduced length is 600 mm. Since the flange of the HP pile is reduced, this connection type is expected to reduce the stiffness of the connection, the reduced stiffness is expected to the more flexible behavior of the pile-to-pilecap connection.
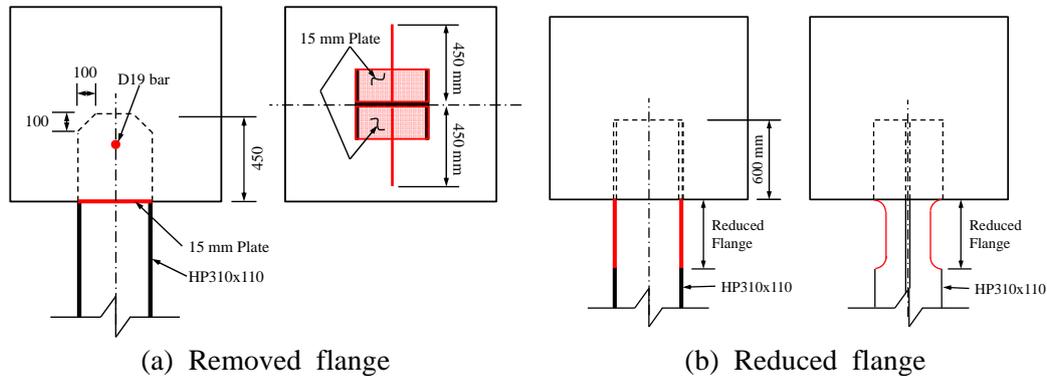

(a) Removed flange   (b) Reduced flange

Fig. 4-12 Detail of removed flange and reduced flange connection type

Details of the hole connection type and the extended hole connection type are shown in Fig. 4-13. In hole connection type and extended hole connection type, to make air gaps artificially between the H-pile and the pilecap, the polystyrene can be used to fill the air gaps. When curing of the concrete, the polystyrene can be embedded in the pilecap to make air gap. In numerical model, the polystyrene is not considered since the polystyrene has a very small stiffness compared to other construction materials. In the hole connection type, there are 4 air gaps at the edge of the flange to reduce the stress concentration since the crack is iniciated from the edge of flanges. Furthermore, this connection type is expected to more flexible behavior due to the polystyrene. In the extended hole connection type, the concrete surface of the pilecap which is contacting to the web was removed. This model is expected to allow the displacement due to the spacing between the H-pile and the concrete of the pilecap. Delayed contact time due to the allowed displacement is expected to increase flexible behavior.
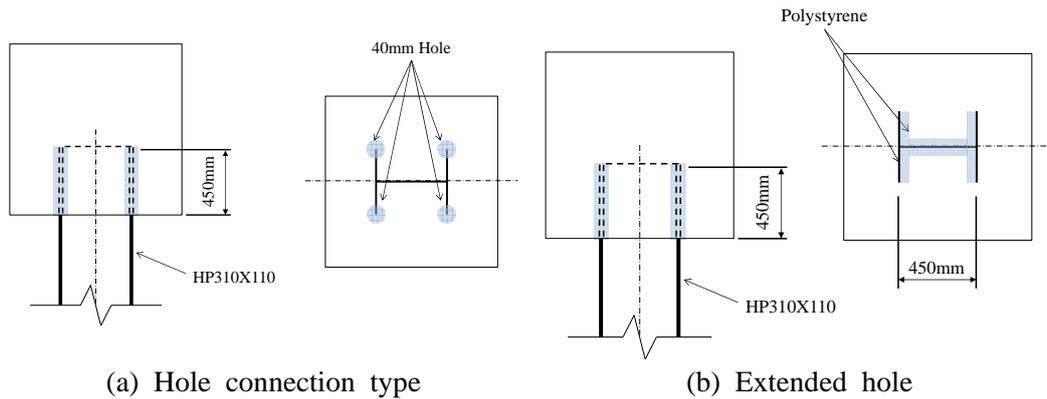
(a) Hole connection type　　　　(b) Extended hole

Fig. 4-13 Detail of hole connection type and extended hole connection type

The PHC connection type is shown in Fig. 4-14(a). The 65 mm thick PHC pile is used instead of the HP pile in this connection type and a 3 mm thick 600 mm length steel pipe is present at the bottom of the pilecap. Half of the length of the steel pipe is embedded within the pilecap and the other part was on top of the PHC pile. This steel pipe within the embedded region has shear stud to prevent down-drag from the pilecap, also plays the role in connecting the PHC and the pilecap. This connection type is expected to absorb all the energy that the abutments would receive due to flexible performance. A reduced flange with spiral rebar connection type is shown in Fig. 4-15(b). This connection type is a combination of the spiral rebar and the reduced flange connection type. The spiral rebar is an effective connection type to control crack propagations, increase structural integrity of the connection, and reduced flange increase flexible behavior. This connection type is expected to show resist crack propagation after flexible performance due to reduced flanges.

The slot connection type is shown in Fig 4-15. Slot connection type is similar to the extended hole details. This connection type is expected to flexible behavior due to the allowed displacement.
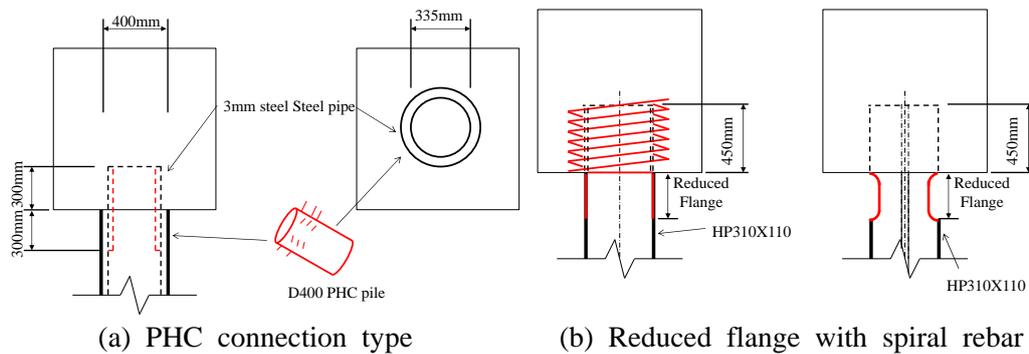
(a) PHC connection type   (b) Reduced flange with spiral rebar

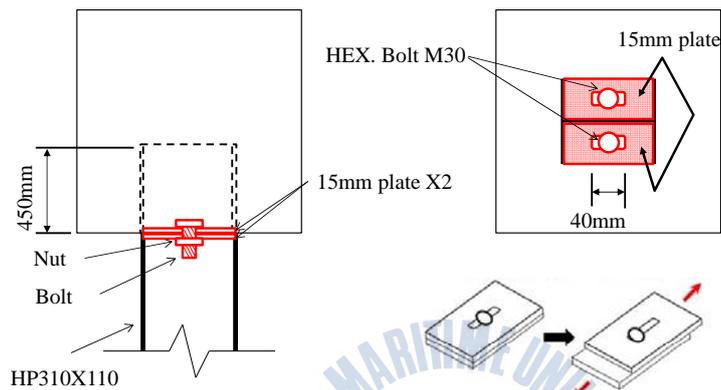Fig. 4-14 PHC connection type and reduced flange with spiral rebar connection type

Fig. 4-15 Detail of slot connection type

4.3.3 Obtained Results of Increased Stiffness Connection Types

The crack patterns and the maximum rebar stress of the PennDOT connection type were shown in Fig. 4-16. The maximum reaction force was 94 kN at a displacement of 61mm. The crack initiation and propagation patterns were similar to RO + TO model. After numerical model, The pilecap body was splitted into two pieces due to cracks. Maximum stress of steel rebar was approximately 33 MPa, It was only 11% of f_y. The complete pilecap crack was occurred at 61 mm displacement, maximum rebar stresses were 203 MPa, It was 68% of f_y. PennDOT rebar detail is ineffective for mitigating crack initiation and propagation in the pile-to-pilecap connection.
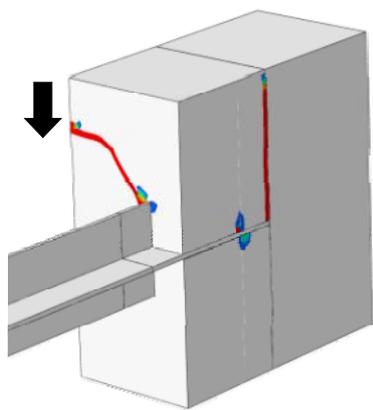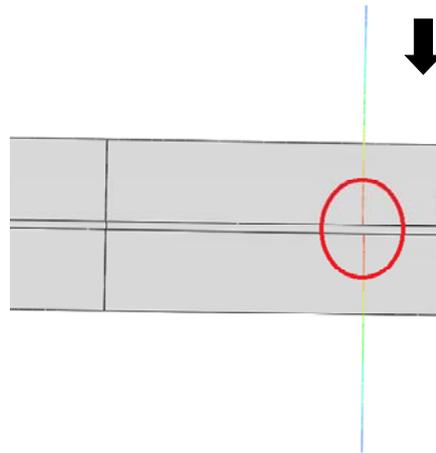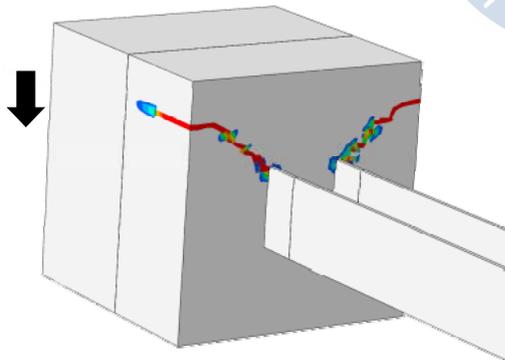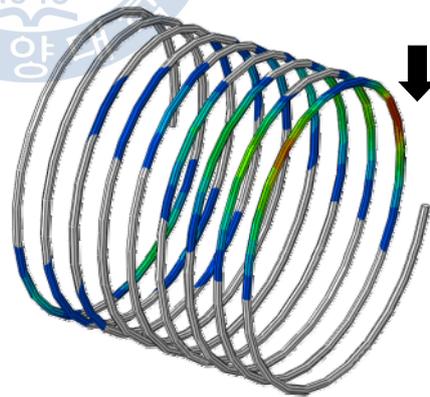
(a) Crack patterns   (b) Maximum rebar stress

Fig. 4-16 Crack patterns and maximum rebar stress of PennDOT

Fig. 4-17 shows the results of spiral rebar. The complete pilecap crack was occurred at a 93 mm displacement. The complete pilecap crack was delayed and occurred at larger displacement due to spiral rebar. The rebar stress was increased up to 352 MPa after pilecap cracking. The study found that the PennDOT detail was not effective in preventing crack propagation, however spiral rebar was effective for increasing the performance of the connection.

(a) Crack patterns   (b) Maximum rebar stress

Fig. 4-17 Crack patterns and maximum rebar stress of spiral rebar connection type

Fig. 4-18 shows the results of HSS tube connection type. First crack was initiated from the corners of the HP pile at 33 mm displacement, and this crack could not propagate due to a HSS tube connection type. Second cracks were occurred at the edge of the HSS tube connection type at 57 mm displacement. Compared to RO + TO model, the HSS tube connection type was not effective due to rounded corner shape of steel tube. The maximum load of HSS tube connection type was 83 kN. It is smaller than RO + TO model 90 kN. Von Mises stress of the steel tube was 49 MPa. It was not failed before second crack, indicating that steel tube was ineffective in the pile-to-pilecap connection.

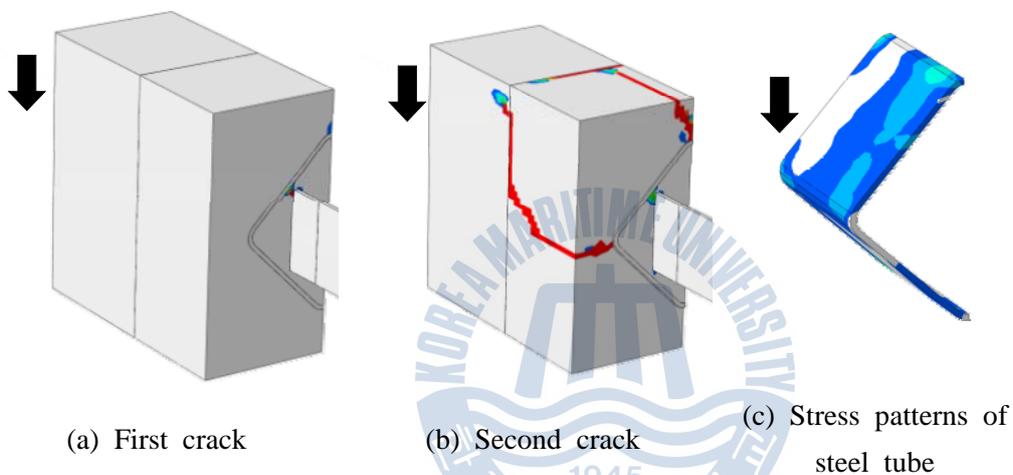(a) First crack   (b) Second crack   (c) Stress patterns of steel tube

Fig. 4-18 Crack patterns and stress patterns of HSS tube connection type

The crack patterns and the plastic strain of the square rebar connection type are shown in Fig. 4-19. The complete pilecap crack was occurred at 71 mm displacement. The maximum load of square rebar connection type was 111 kN, and the rebar was failed. Parametric study of the number of the rebar is presented in the next section.

Fig. 4-20 shows the results of the grid rebar connection type. The maximum reaction force at 70 mm was 108 kN. A plastic strain in the steel rebar occurred

in the loading direction of the rebar. The grid rebar connection type was more effective with respect to reaction force and displacement than the PennDOT connection type (94 kN, 61 mm). An embedded rebar was effective for mitigating crack initiation and propagation. Therefore, it was expected that using more rebars would increase the resistance to crack generation. On the other hand, using too many rebar can decrease the construct ability as compared to the spiral rebar connection type.
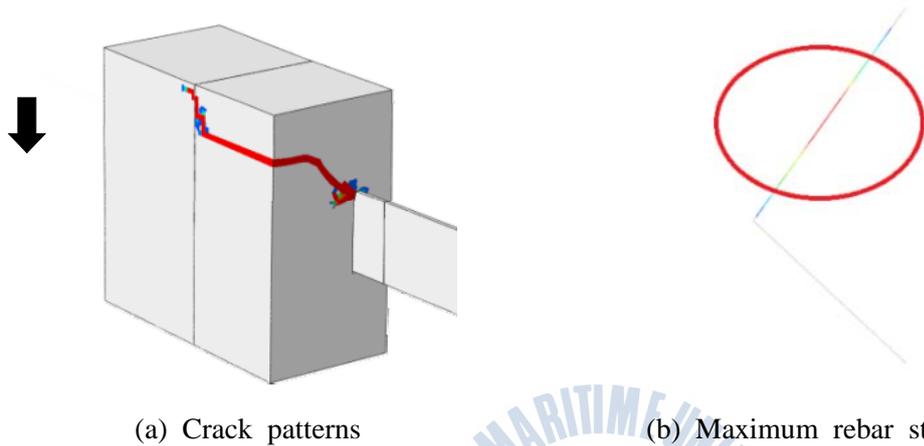

(a) Crack patterns   (b) Maximum rebar stress
Fig. 4-19 Crack patterns and maximum rebar stress of square rebar connection type

4.3.4 Obtained Results from Flexible Connection Types

Crack patterns and plastic strain of the removed flange connection type are shown in Fig. 4-21. A small crack was observed in the middle of the H-pile. The crack was not propagated until 100 mm displacement, and the flexible performance was observed due to plastic hinge (Fig. 4-21(c)). In this connection type, the pilecap was prevented from stress concentration due to the presence of flange. The maximum reaction force at 100 mm was 100 kN. This maximum reaction force was higher than the spiral rebar connection type. This indicated that the energy absorption capacity of removed flange connection type was better than the other connection types. An embedded rebar in the pilecap yielded 98 mm displacement. The plastic strain of the rebar was 0.00016. This indicated that the plastic hinge
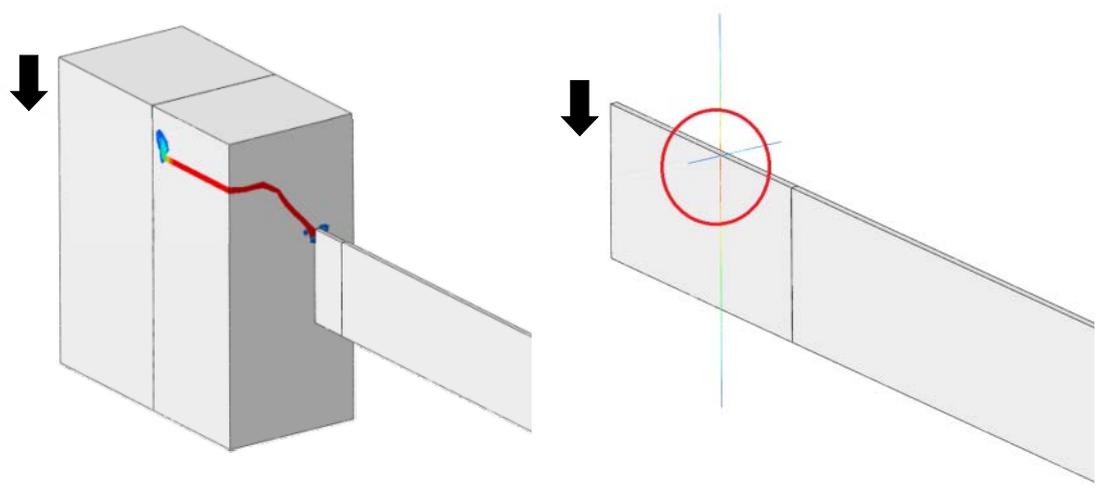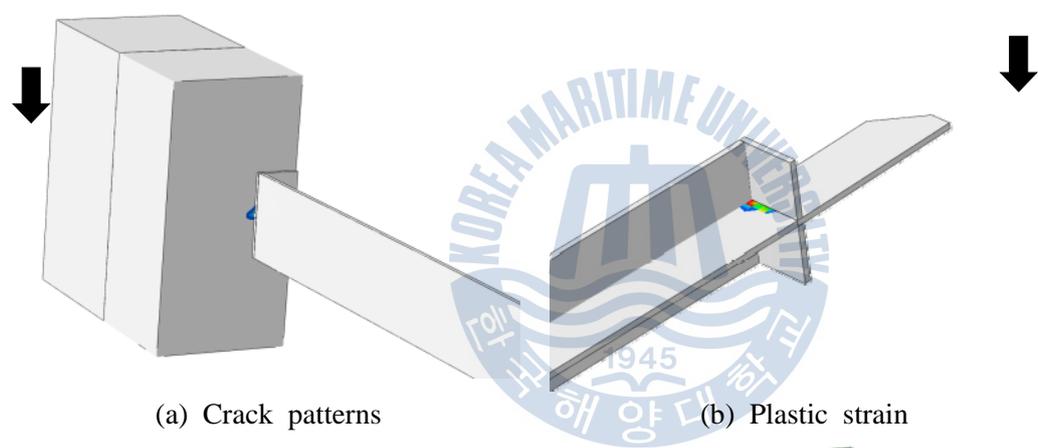
reduced the pile stiffness.

(a) Crack patterns   (b) Plastic strain
Fig. 4-20 Crack patterns and plastic strain of grid rebar connection type

(a) Crack patterns   (b) Plastic strain

(c) Deformation (Scale 20)
Fig. 4-21 Crack patterns and plastic strain of removed flange connection type

Fig. 4-22 shows the results of the reduced flange connection type. The crack was not propagated until 100 mm displacement. The maximum reaction force at the 100 mm displacement was 120 kN. A plastic hinge was also observed in reduced flanges, flexible performance was observed (Fig. 4-22(c)).
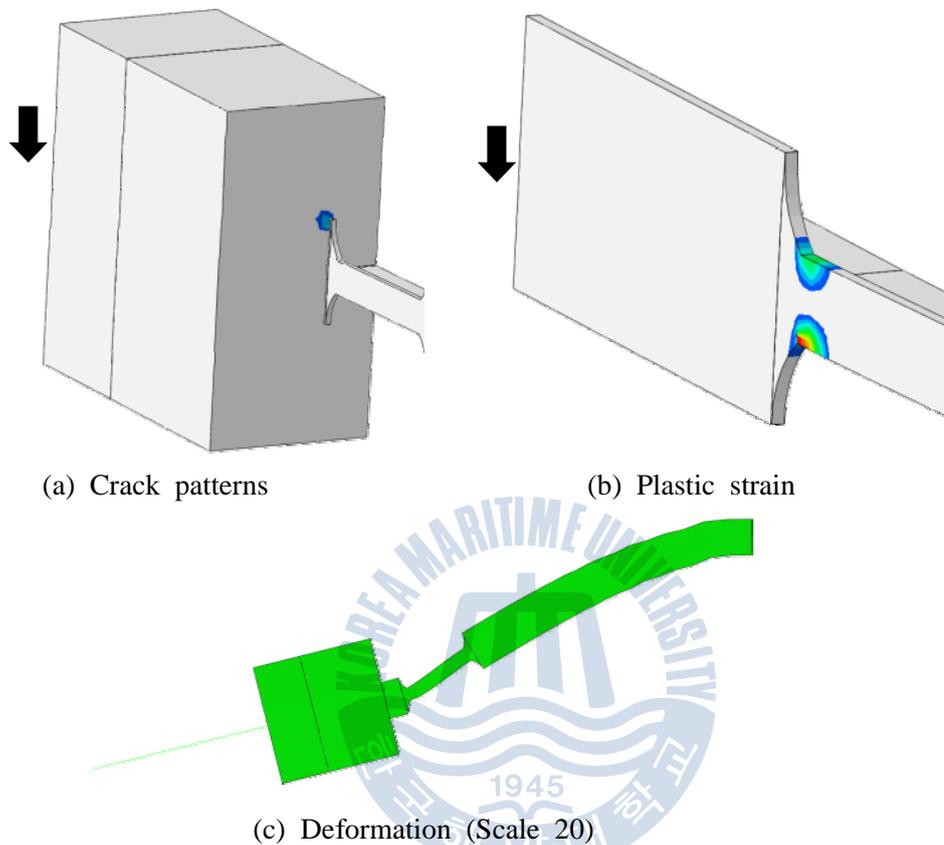

(a) Crack patterns   (b) Plastic strain

(c) Deformation (Scale 20)

Fig. 4-22 Crack patterns and plastic strain of reduced flange connection type

Fig. 4-23 shows the results of the hole connection type. The crack patterns of the concrete was shown in Fig. 4-23(a) and stress patterns of H-pile was shown in Fig. 4-23(b). The maximum reaction force at 57mm was 85 kN. Hole connection type was expected to the flexible performance, however the flexible performance did not observe due to the resistance of the web. Comparing with RO + TO, hole connection type was inefficient to improve the performance of the pile-to-pilecap connection.

Collection

(a) Crack patterns   (b) Stress contour of HP pile

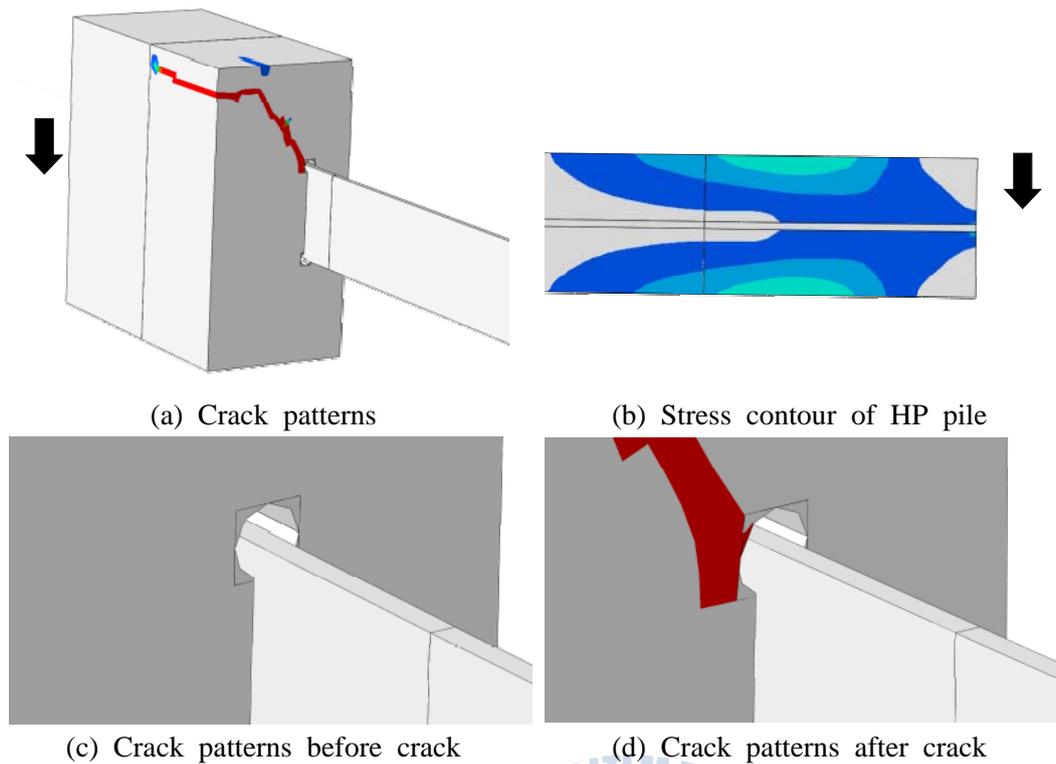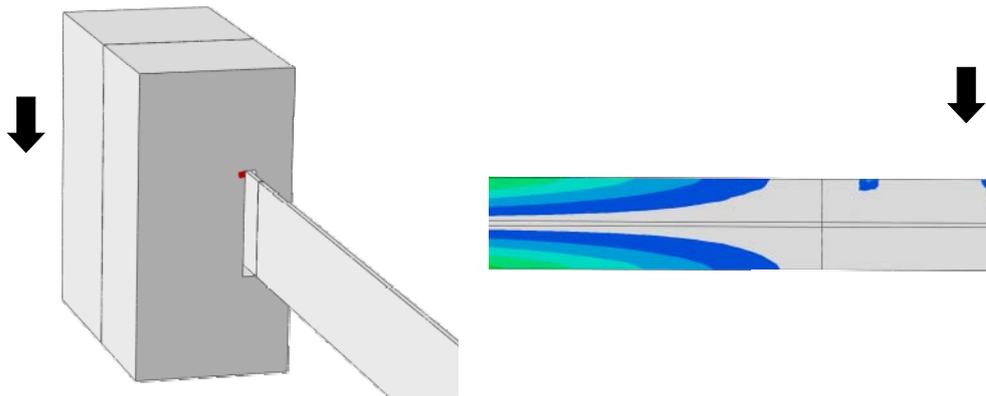(c) Crack patterns before crack   (d) Crack patterns after crack
Fig. 4-23 Crack patterns and stress contour of hole connection type
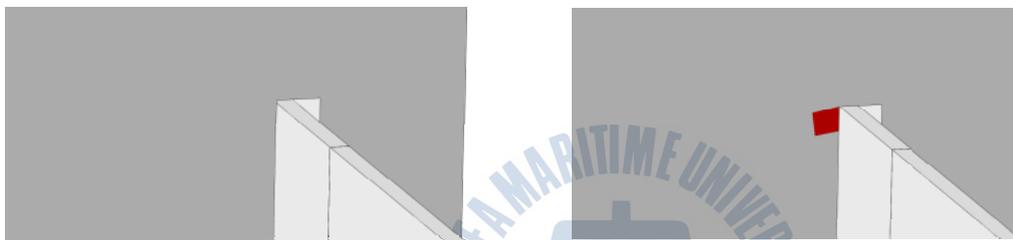
Fig. 4-24 shows the results of the extended hole connection type. During construction, the air gap can be filled with polystyrene. The contact stresses were not transferred to the pilecap before contact occurred due to air gaps. Therefore, the reaction force was approximately zero until a 20mm displacement was reached. After 20 mm displacement, small crack was occurred due to the contact force between HP pile and pilecap. The negligible crack was occurred until 100 mm displacement. This indicates that the proposed extended hole connection type could be used for mitigating cracks in the pilecap. The displacement of this study could be readjusted instead of 20 mm to allow a larger displacement. However, too much large gap could cause instability of the connection and a construct ability. The further study should be conducted to find optimized hole. The maximum stress of the H-pile was 55.9 MPa at the contact area. The maximum stress was lower than yield stress of the steel rebar (400 MPa). The plastic strain of the H-pile was

occurred at the fixed location. The crack of concrete was not propagated until the displacement of 100 mm.

(a) Crack patterns

(b) Stress contour of H-pile before contact

(b) Crack patterns before contact   (c) Crack patterns after contact
Fig. 4-24 Crack patterns and stress contour of extended hole connection type

Fig. 4-25 shows results of the PHC connection type. The maximum reaction force was 30 kN at a displacement of 25 mm. This connection type was inefficient compared to other connection types. The plastic strain was not occurred in pilecap in this model. However, The plastic strain was occurred the edge of the bottom fixed location. The contact force did not transfer to pilecap since the moment and stresses were concentrated in fixed location. After improve the detail of PHC connection type, the further study should be conducted analysis.
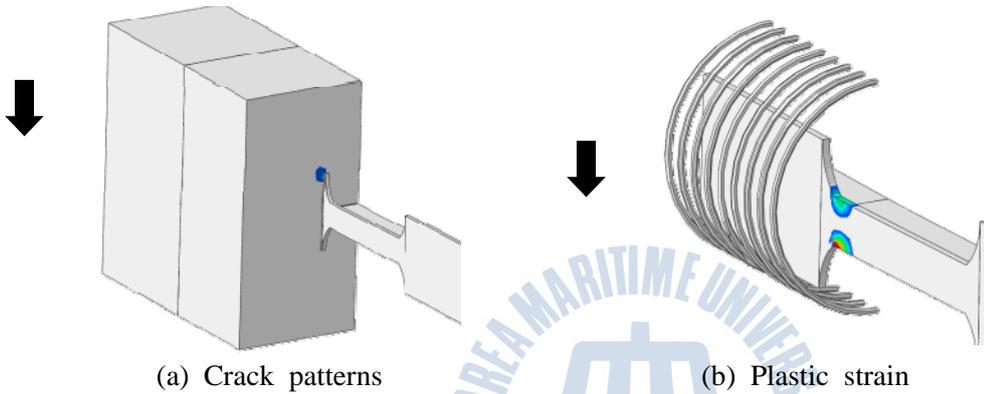
Fig. 4-26 shows the results of the reduced flange with spiral rebar connection type. The flexible behavior was observed (Fig. 4-26(c)), furthermore small crack initiation was observed near the H-pile in the pilecap but crack propagation was

not occurred. The maximum reaction force was similar to the removed flange connection type at a displacement of 100mm. This indicated that the influence of spiral rebar was small when spiral rebar was used with the reduced flange. A plastic hinge was also formed at the pile as shown in Fig. 4-26(b).
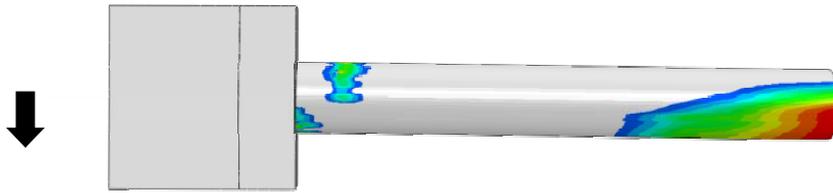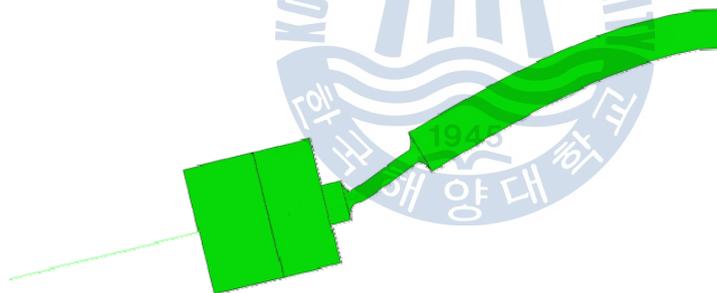

(a) Crack patterns
Fig. 4-25 Damaged area of PHC connection type

(a) Crack patterns   (b) Plastic strain

(c) Deformation (Scale 20)
Fig. 4-26 Crack patterns and plastic strain of reduced flange with spiral rebar connection type

Fig. 2-27 shows the results of the slot connection type. The allowed displacement was 20 mm due to 40 mm slot. The reaction force was approximately zero until a 20 mm displacement was reached without any stress transferring to the concrete

pilecap. After the displacement of 20 mm, a contact was formed between the bolts and the slot surface and the contact forces started to transfer. Fig. 4-27(b) shows the deformed shape after the contact. A plastic strain occurred at the slot connections. The crack initiation occurred at a displacement of 36 mm. However, the crack did not propagate until a displacement of 100 mm occurred.
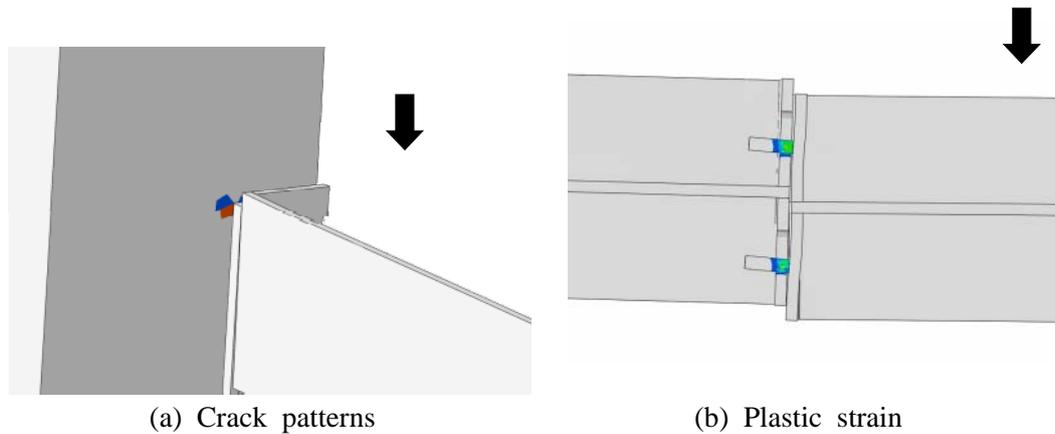

(a) Crack patterns   (b) Plastic strain
Fig. 4-27 Crack patterns and plastic strain of slot connection type

4.3.5 Comparison of Load-displacement Curves

The maximum displacement, the reaction force and the calculated energies are presented in Table 1. Fig. 4-28 shows load-displacement curves of PennDOT, square rebar, grid rebar, HSS tube connection type and spiral rebar connection type. The performance of the PennDOT rebar detail shows the same performance as to RO + TO. This data indicates that PennDOT connection type is not effective to control the crack propagation. The grid rebar connection type shows the same performance as to the square rebar connection type. The grid rebar and square rebar exhibits higher strength and displacement compared to RO + TO model. The concrete crack failure of the HSS tube connection type occurs at a displacement of 56mm. The connection failure occurs even earlier than the RO + TO model. This indicates that the HSS tube connection type can not prevent crack propagation and allow a large reaction force. The spiral rebar connection type shows 1.6 times higher strength and displacement compared to RO + TO. Concrete cracks

generation are delayed and strength is increased significantly due to spiral rebar. The energy absorption is increased to 6371 kN-mm compared to RO + TO model (2610 kN-mm). However, the stiffness is not changed.
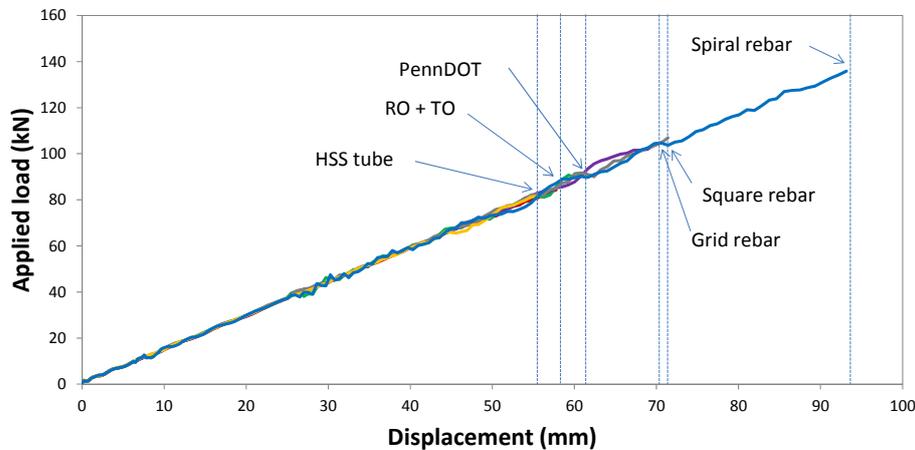

Fig. 4-28 Load-displacement curves obtained from increased stiffness connection types

The results of RDF (Reduced flange) connection type, RMF (Removed flange) connection type, PHC connection type, slot connection type, hole connection type, extended hole connection types, and reduced flange with SR (Spiral Rebar) connection type are shown in Fig. 4-29. RMF connection type, RDF connection type and RDF with SR connection type show no crack propagation and less stiffness compared to other connection types. Also, The larger displacement are obtained. RMF connection type showed a small energy since a small reaction force is generated due to the effect of the removed flange. The maximum reaction force at 100 mm displacement is 100 kN. The D19 rebar which is inserted for resisting the downwards force from the pile start to yield at a displacement of 98 mm. The plastic strain of D19 is occurred at 100 mm displacement. RDF connection type and RDF with SR (spiral rebar) connection type shows the same performance each other. The energies of the RDF connection type and the RDF with SR connection type are 6694 and 6699 kN-mm. This indicated that the reduced flange is not efficient with spiral rebar. The RMF connection type shows small energy absorption

– 44 –

capacity, this indicates that the performance of RMF connection type is improved. The small reaction force is generated in the RMF connection type compared to the RDF connection type and the RDF with SR connection type, this indicates that removed flange is more efficient than reduced flange to flexible performance of pile-to-pilecap connection. The slot connection and the extended hole connection type shows no reaction forces up to a displacement of 20 mm due to extended holes and slotted holes. After contact occurred, the reaction forces significantly and rapidly increased. The performance of the hole connection type shows the same performance as to RO + TO model. This indicates that the hole connection type is inefficient compared to other connection types. The PHC connection type shows small strength and displacement due to damaged bottom surface of pile.
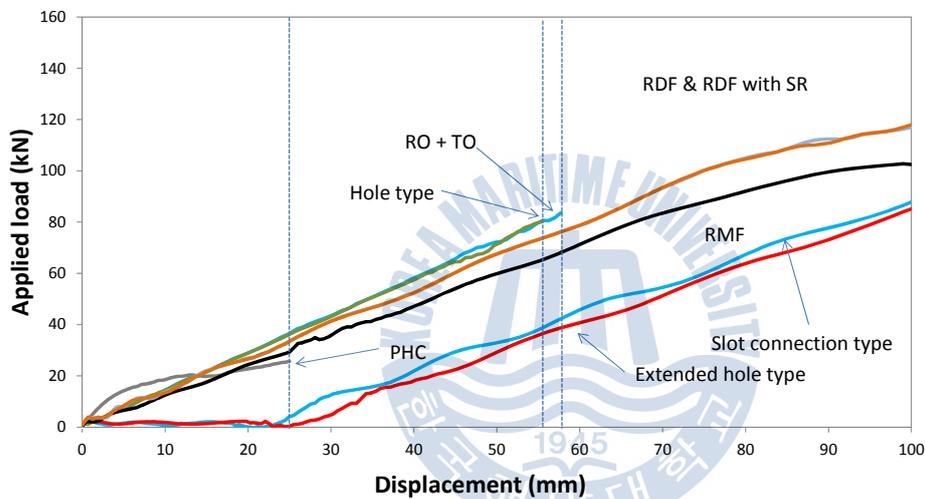

Fig. 4-29 Load-displacement curves obtained from flexible connection types

Table 1 Obtained results from all connection types

Connection type	Maximum displacement (mm)	Reaction Force	Energy (kN-mm)
TO	14	64	439
RO	22	49	539
RO + TO	58	90	2610
PennDOT	61	94	2827
Square rebar	71	111	3829
Grid rebar	70	108	3764
HSS tube	56	83	2303
Spiral rebar	93	137	6371
Removed flange	100	100	5940
Reduced flange	100	120	6694
Reduced flange with spiral rebar	100	120	6699
Hole	57	85	2446
Extended hole	100	95	3987
Slot	100	96	4022
PHC	25	30	471

4.4 Parametric Study

In this section, conducted parametric study of the spiral rebar and the square rebar are described. Conducted parametric study is rebar size, rebar diameter, pitch size and the number of rebar.

4.4.1 Parameter of Parametric Study

The parametric studies of the spiral rebar and the square rebar are conducted. The conducted parametric studies on the spiral rebar and the square rebar are shown in table 2 and table 3.
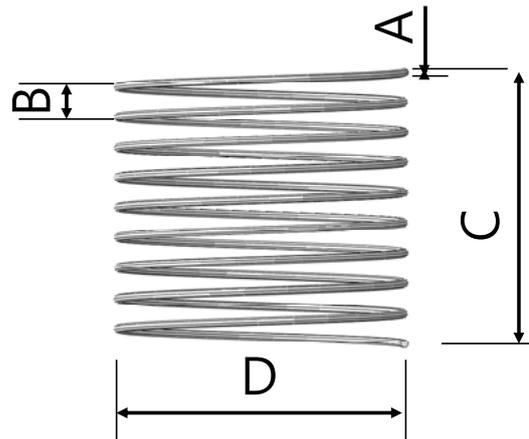
Fig. 4-30 Parameter of spiral rebar

Table 2 Parameter of spiral rebar

(A) Diameter (mm)	(B) Pitch (mm)	(C) Length (mm)	(D) Width (mm)
9.53	50	450	470
12.7	50	450	470
25.4	50	450	470
12.7	25	450	470
12.7	100	450	470
12.7	50	450	520
12.7	50	450	570
12.7	50	450	670
12.7	50	450	470 (bottom) - 670 (top)

Table 3 Parameter of square rebar

Diameter (mm)	Pitch (mm)	The number
12.7	0	1
12.7	120	2
12.7	120	4
12.7	50	8

4.4.2 Results of Parametric Study

The results of developed connection types regarding a parameter of pitch spacing have been shown in Fig. 4-31. A smaller pitch spacing shows a increased reaction force and a increased displacement compared to larger pitch spacing. The reaction force with a 50 mm pitch spacing increase up to 14.4% compared to a 100 mm pitch spacing. The applied load of a 25 mm pitch spacing increase up to 3.2% compared to a 50 mm pitch spacing. The obtained results indicates that pitch spacing should be considered in design code.
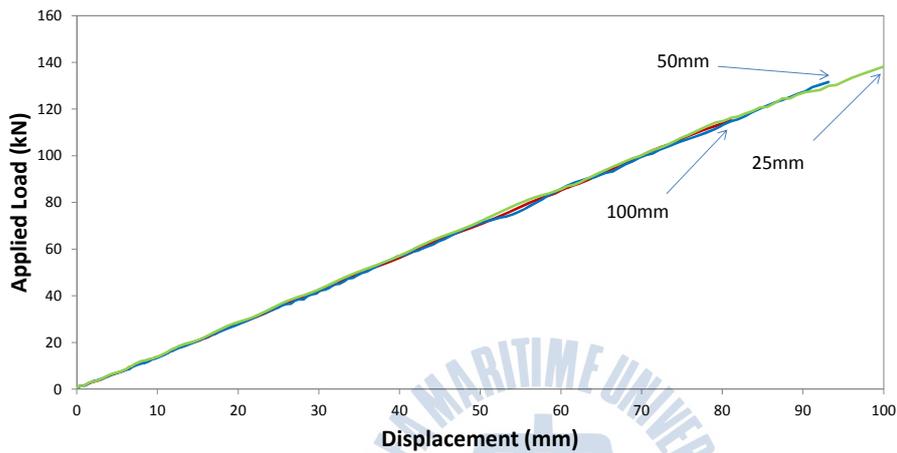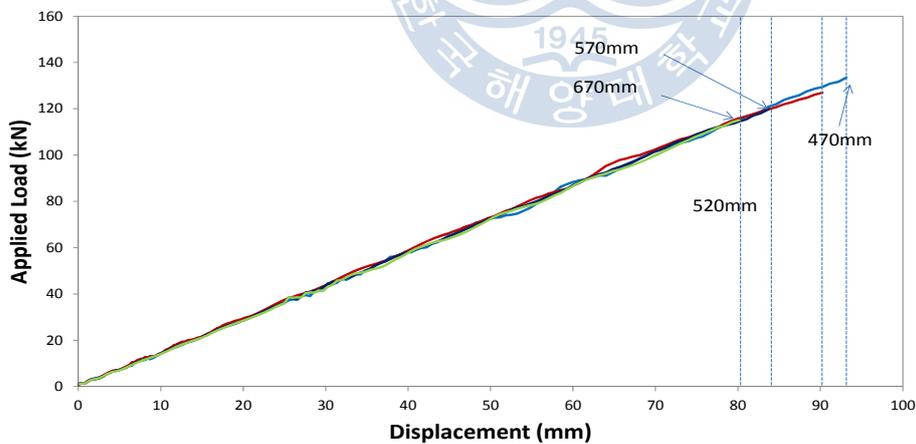

Fig. 4-31 Parametric study on pitch spacing of spiral rebar

The results of developed connection types regarding a parameter of diameter have been shown in Fig. 3-32. A rebar with larger diameter shows increased reaction force and a increased displacement compared to smaller diameter. The reaction force of 12.7 mm diameter increase up to 10.2% compared to the 9.53 mm diameter. The reaction force of 25.4 mm diameter increase up to the 12.7 mm diameter 0.8%. The largest increased in the diameter is 12.7 mm from 9.53 mm. The obtained results shows that the diameter should be considered in design code.
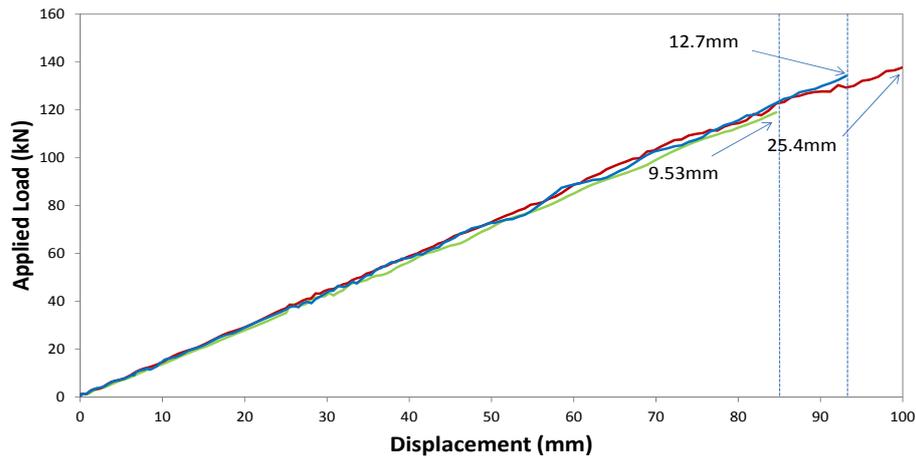
Fig. 3-32 Parametric study on diameter of spiral rebar

The results of developed connection types regarding a parameter of width have been shown in Fig. 4-33. A wider width shows a smaller reaction force and a smaller displacement compared to narrow width. The reaction force of 570 mm width increase up to 5.6% compared to the 670 mm width. The reaction force of 520 mm width increase up to 1.7% compared to the 570 mm width. The reaction force of 470 mm width increase up to 8.9% compared to the 520 mm width. The obtained results indicates that width of spiral rebar should be considered in design code.

Fig. 4-33 Parametric study on width of spiral rebar

The results of developed connection types regarding a parameter of asymmetry spiral have been shown in Fig. 4-34. The asymmetry spiral rebar shows the same performance compared to 470 mm width. The reaction force of 470 mm width increase up to 2.1% compared to the asymmetry spiral rebar. This obtained result indicats that bottom width of spiral rebar should be considered in design code to improve the performance of pile-to-pilecap connection.
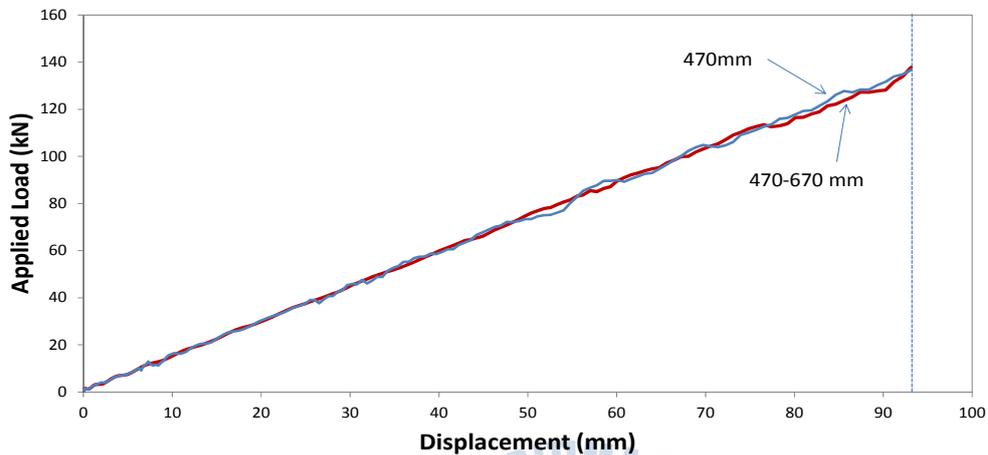

Fig. 4-34 Results of asymmetry spiral rebar

The results of developed connections regarding the quantity of square rebar have been shown in Fig. 4-35. The performance with one square rebar shows ineffective performance. The performance with two rebars shows the same behavior with the four rebars. This indicates that a embedded rebar in the top do not improve the performance of pile-to-pilecap connection. The eight rebars show the largest applied force and displacement compared to other connections. The results indicates that the quantity of square rebar should be considered in design code.
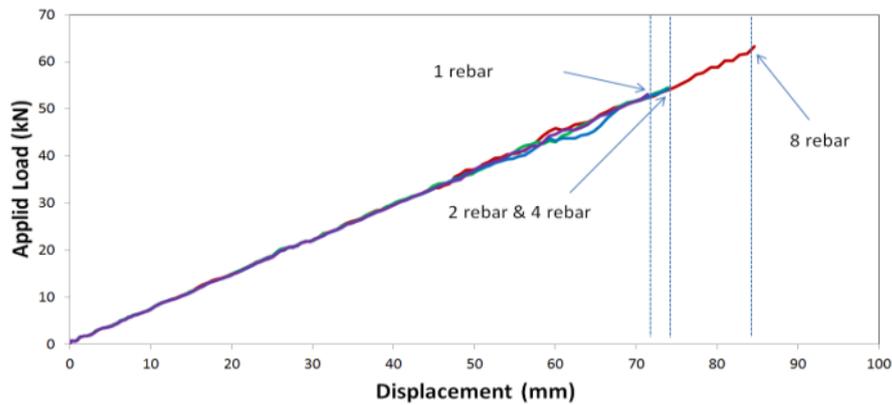
Fig. 4-35 Parametric study on quantity of square rebar

The results of calculated energies are shown in Table 4 and Table 5. A larger diameter, a smaller pitch spacing and a smaller width shows a larger energy absorption capacity. A asymmetry spiral rebar shows similar energy absorption capacity compared with 470 mm width. The energy absorption capacity with eight rebars increased up to 31.2% compared to four rebars. The shape of spiral rebar and the number of rebar should be considered in design code due to different energy absorption capacity.

Table 4 Results of parametric study of spiral rebar

(A) Diameter (mm)	(B) Pitch (mm)	(C) Length (mm)	(D) Width (mm)	Maximum displacement (mm)	Reaction Force (kN)	Energy (kN-mm)
9.53	50	450	470	100	126	5353
12.7	50	450	470	93	137	6371
25.4	50	450	470	100	140	7382
12.7	25	450	470	100	144	7400
12.7	100	450	470	81	122	4934
12.7	50	450	520	90	128	6058
12.7	50	450	570	84	125	5249
12.7	50	450	670	80	119	4911
12.7	50	450	470 (bottom) - 670 (top)	93	142	6447

Table 5 Parametric study results of square rebar

Diameter (mm)	Pitch (mm)	Number	Maximum displacement (mm)	Reaction Force (kN)	Energy (kN-mm)
12.7	0	1	71	56	1915
12.7	120	2	74	55	2034
12.7	120	4	74	56	2042
12.7	50	8	85	65	2681

4.5 Superstructure Model

In this section, the superstructure was modeled with a consideration of load-displacement data obtained from previous pile-to-pilecap connection models. Thermal expansion of the superstructure was considered and damaged elements were counted depending on the pile-to-pilecap connections types.

4.5.1 Development of Superstructure Model

In order to compare the performance of each model of pile-to-pilecap connections, another numerical model is developed. The details of superstructure are shown in Fig. 4-36, 4-37 and 4-38. The 2D numerical model is developed in order to confirm the performance of superstructure with pile-to-pilecap connections. The abutment is a cohesive element. Generally, cohesive elements are useful in modeling adhesives, bonded interfaces, gaskets and rock fractures. The constitutive responses of these elements are based on specific applications and certain assumptions about the deformation, and the stress states are appropriate for each application area. The nature of the mechanical constitutive response can be broadly classified based on Abaqus 6.13 manual. In the superstructure model, the cohesive material properties were determined based on the results of pile-to-pilecap connections. The girder in the model is an elastic material, therefore the elements of girder can not show any plastic behavior. The slab is a concrete damaged plasticity model. The D19 longitudinal rebars are placed in the top of the slab with the spacing of 228.6 mm, the D19 longitudinal rebars are placed in the bottom of the slab with the spacing of 457.2 mm. The pairs of D16 stud rebar are placed up

to 15.24 m from the edge along the length of the girder with the spacing of 300 mm. Likewise, the pairs of D16 stud rebar are placed between 15.24 m and 45.72 m along the length of the girder with the spacing of 450 mm. The temperature load is also considered in this numerical model. At the bottom of the slab, the temperature is 0℃, and on the top of the slab the temperature is 15℃. The compression strength of the bridge is shown in Table 6. Obtained results, the evaluation was conducted and compare with each model.
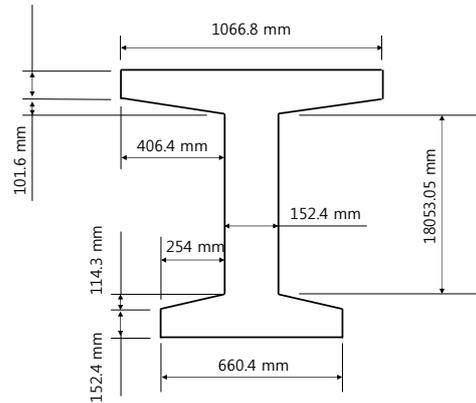
Fig. 4-36 Detail of girder
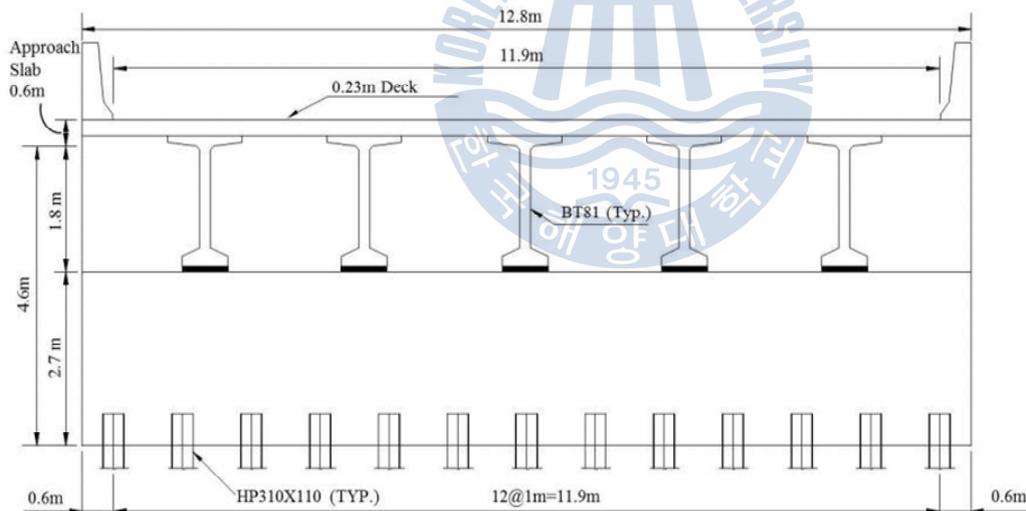
Fig. 4-37 Cross sectional view of the numerical model
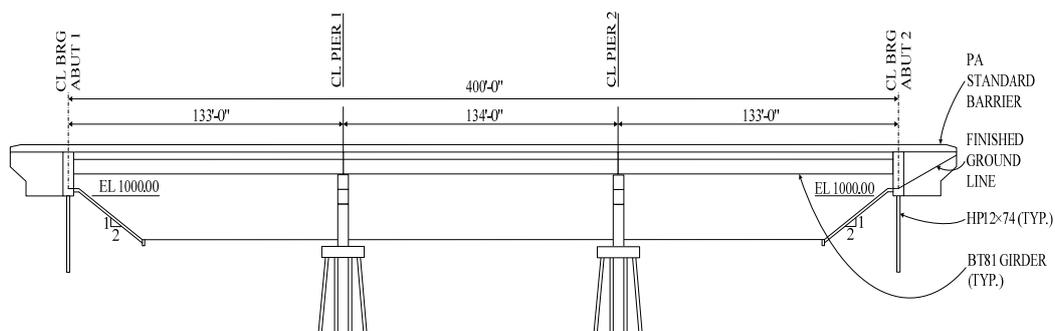
Fig. 4-38 Profile of the numerical model

Table 6 Compression strength of bridge

Deck slab, Backwall	27.6 MPa
Girder	55.2 MPa
Abutment	20.7 MPa

4.5.2 The Results of Increased Stiffness Superstructure Model

Fig. 4-39 shows crack patterns of superstructure model with RO + TO. The crack was occurred at the edge of slab and a support. A main crack occurred between a girder and a slab. This indicated that when a 100 mm displacement occurred in the 121.92 m bridge, the girder and slab were separated. The number of damaged elements were 1205.
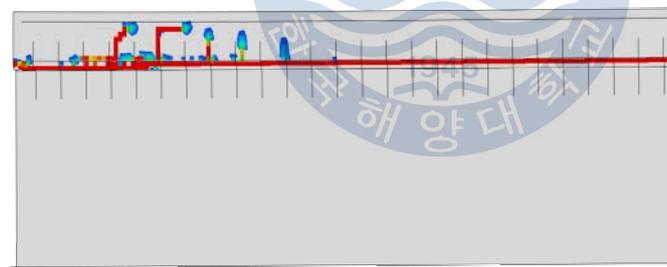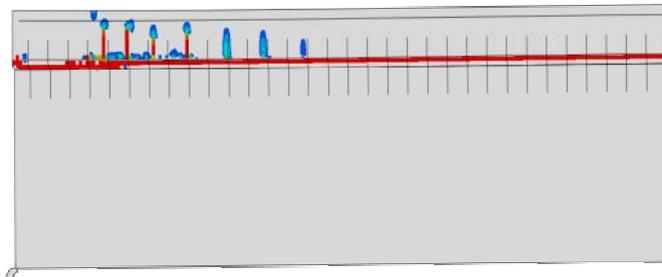

(a) Crack patterns at the edge
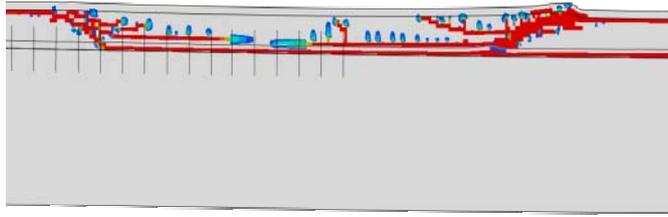
(b) Crack patterns in mid-span
Fig. 4-39 Crack patterns of RO + TO

Fig. 4-40 shows crack patterns of superstructure with PennDOT. The number of damaged elements were 1187. Crack patterns were similar with RO + TO due to similar stiffness. However, obtained pile-to-pilecap connection results, the complete pilecap crack with RO +TO was occurred at 58 mm displacement, the complete pilecap crack with PennDOT connection type was occurred at a 61 mm displacement. Therefore, RO + TO showed inefficient performance compared to PennDOT connection type.
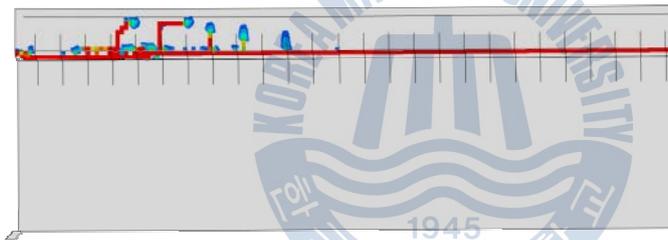
(a) Crack patterns at the edge
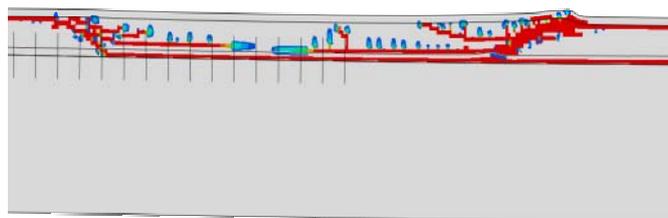
(b) Crack patterns in mid-span
Fig. 4-40 Crack patterns of PennDOT connection type

Fig. 4-41 shows the crack patterns of superstructure with square rebar connection type. The crack patterns was similar with RO + TO. The number of damaged elements were 999, which was decreased compared to RO + TO. The square rebar connection type showed better performance compared to RO + TO.
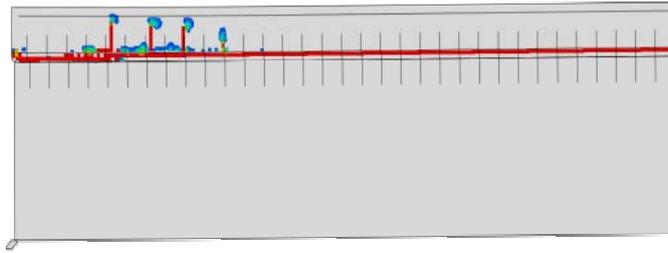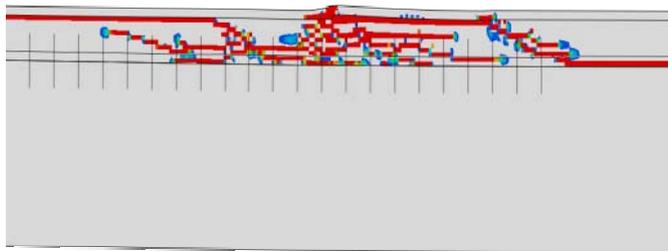

(a) Crack patterns at the edge
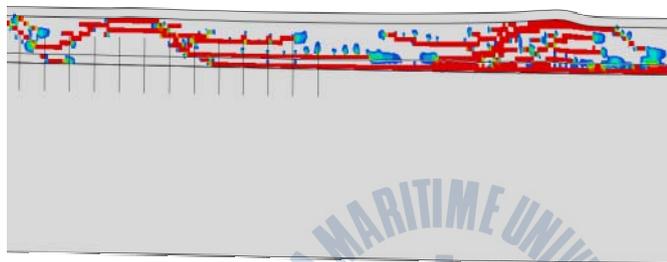
(b) Crack patterns in mid-span
Fig. 4-41 Crack patterns of square rebar connection type

Fig. 4-42 shows crack patterns of superstructure with grid rebar connection type. The number of damaged elements (932) decreased compared to RO + TO (1205). Furthermore, a main crack length which was between girder and slab was decreased compared to the RO + TO. However, a main crack length between the girder and the slab was not decreased compared to other connection types, this indicated that grid rebar connection type was inefficient to improve the performance of the superstructure.
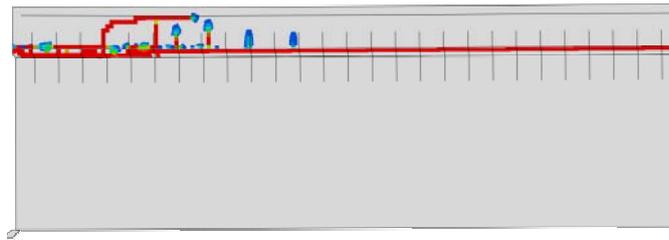
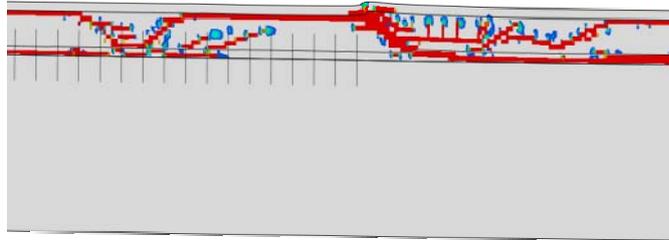(a) Crack patterns at the edge

(b) Crack patterns in mid-span
Fig. 4-42 Crack patterns of grid rebar connection type

Fig. 4-43 shows the crack patterns of superstructure with HSS tube connection type. At the edge, crack patterns were similar with RO + TO model due to similar stiffness. Additionally, the number of damaged elements (1216) were similar with RO + TO model (1205). This results indicated that HSS tube connection type is not improved the performance of the pile-to-pilecap connection.

Crack patterns of superstructure with spiral rebar connection type are shown in Fig. 4-44. Crack patterns, a main crack length and number of damaged elements (863) decreased, as compared to the RO + TO model due to increased stiffness. This results indicated that the spiral rebar was efficient to improve the behavior of superstructure.
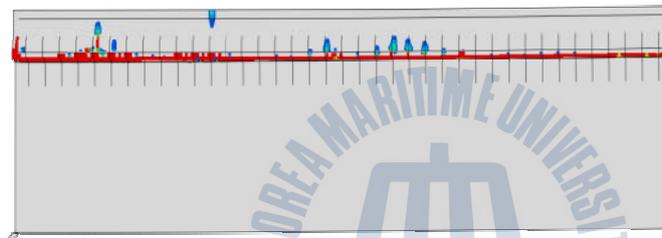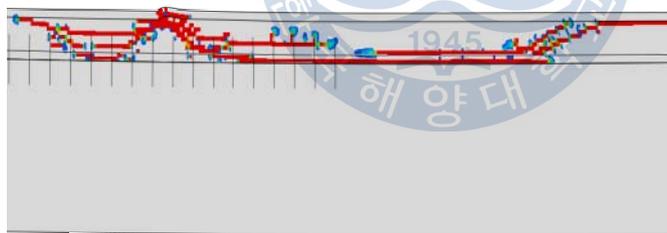
(a) Crack patterns at the edge

(b) Crack patterns in mid-span
Fig. 4-43 Crack patterns of HSS tube connection type

(a) Crack patterns at the edge

(b) Crack patterns in mid-span
Fig. 4-44 Crack patterns of spiral rebar connection type

4.5.3 The Results of Flexible Superstructure Model

Fig. 4-45 shows the results of the RMF connection type. The number of damaged elements was 882. The crack length between the girder and the slab was

shorter than that in the RO + TO model. This results indicated that the removed flange reduced the crack propagation of superstructure, therefore, removed flange is efficient model.

Crack patterns of the superstructure with reduced flange were shown in Fig. 4-46. Crack patterns were similar to RO + TO model, however damaged elements (827) were decreased compared to RO + TO model (1205). This indicated that reduced flange improve the performance of the superstructure due to the flexible behavior. The flexible models were more efficient than the increased stiffness models.

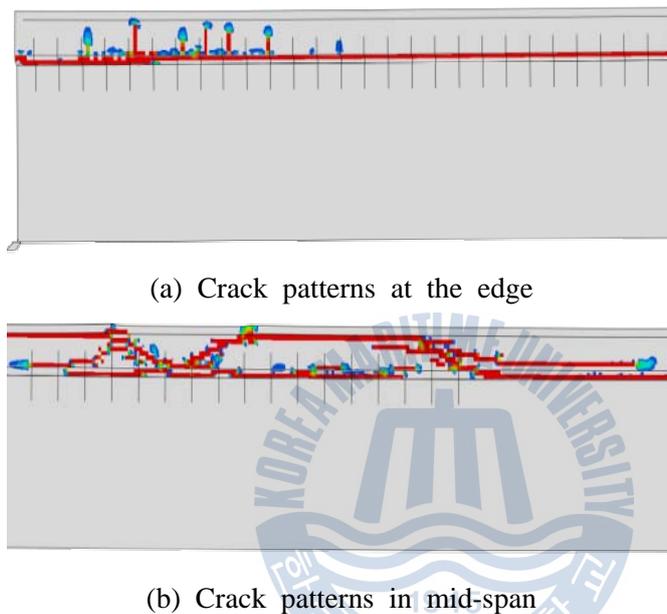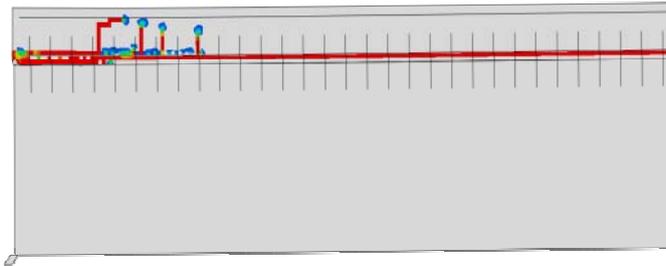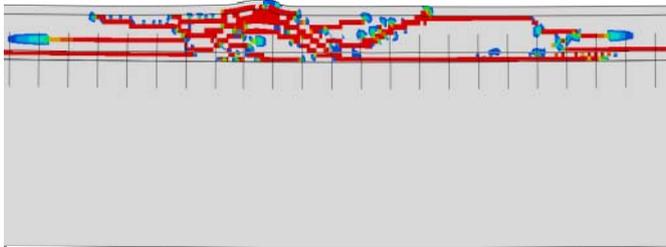(a) Crack patterns at the edge

(b) Crack patterns in mid-span
Fig. 4-45 Crack patterns of removed flange connection type

Crack patterns of the superstructure with reduced flange with spiral rebar are shown in Fig. 4-47. The number of damaged elements was 827. The performance of the superstructure was similar to that of RDF connection type due to similarity in stiffness. Additionally, the crack patterns and crack length were similar with RO + TO model. However, the number of damaged elements were decreased flexibility in the behavior. Therefore, RDF connection type with spiral rebar increased the performance of the superstructure due to flexible behavior.
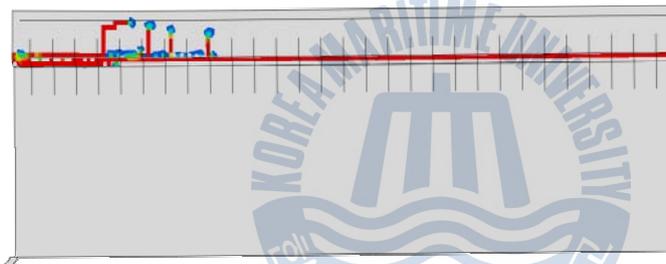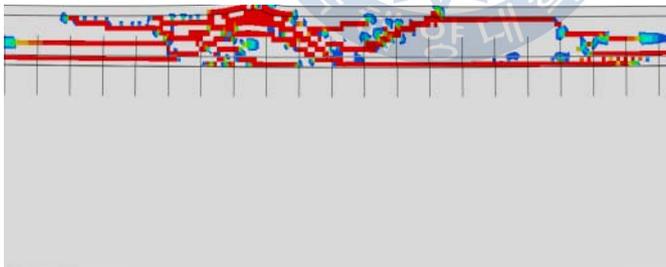
(a) Crack patterns at the edge

(b) Crack patterns in mid-span
Fig. 4-46 Crack patterns of reduced flange connection type

(a) Crack patterns at the edge

(b) Crack patterns in mid-span
Fig. 4-47 Crack patterns of reduced flange with spiral rebar connection type

Fig. 4-48 shows the crack patterns of superstructure with the hole connection

type. The damaged elements (1074) were generated compared to other flexible models, also the larger moment developed on the top of the abutment due to low rotational stiffness. This indicated that the performance of hole was not flexible.

The crack patterns of the superstructure with extended hole connection type are shown in Fig. 4-49. The crack length between the girder and the slab was improved compared to other models due to allowed displacement. The number of damaged elements was 511. This indicated that the flexible model was more efficient in improving the performance of the integral abutment bridge compared to increased stiffness models. The efficiency of the extended hole connection type was increased up to approximately 42% compared to RO + TO model. Therefore, the flexible models could improve the performance of the superstructure compared to increased stiffness models.

(a) Crack patterns at the edge
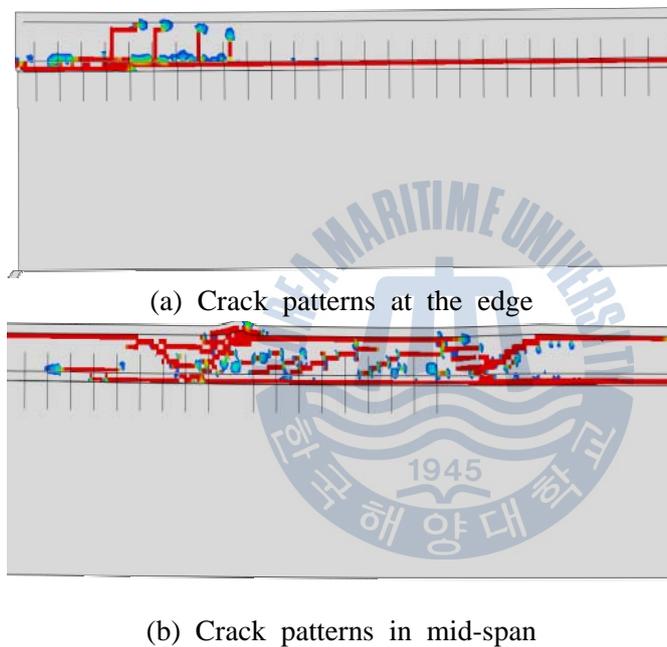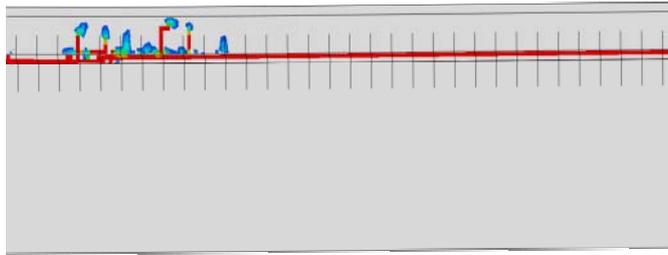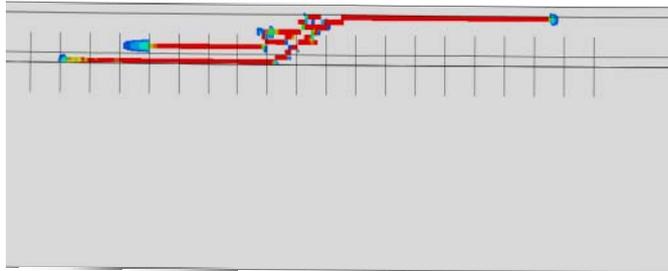

(b) Crack patterns in mid-span
Fig. 4-48 Crack patterns of hole connection type

Fig. 4-50 shows the crack patterns of the superstructure with slot connection. The damaged elements (295) were small compared to other models due to a 40 mm displacement. The results indicated that the allowed displacement connection showed improved performances compared to the increased stiffness connection types.
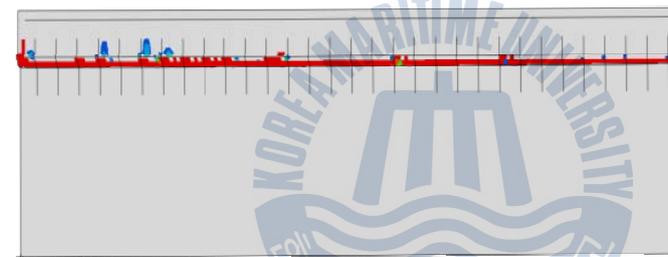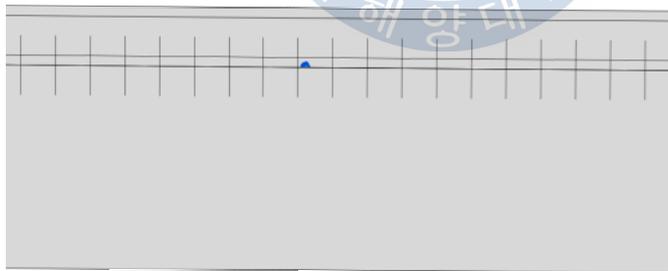
(a) Crack patterns at the edge

(b) Crack patterns in mid-span
Fig. 4-49 Crack patterns of extended hole connection type
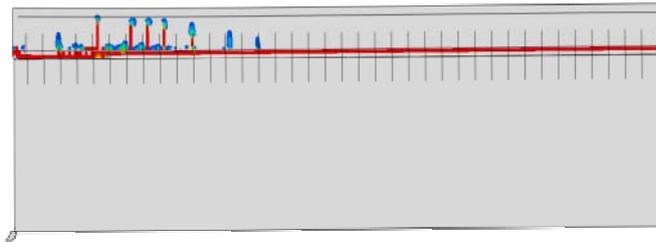

(a) Crack patterns at the edge

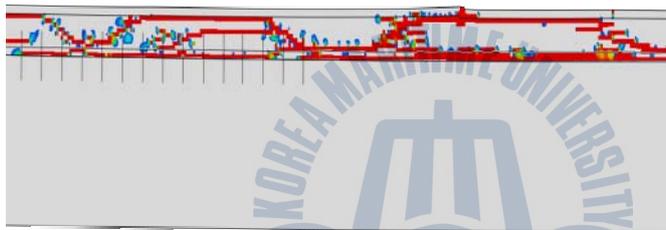(b) Crack patterns in mid-span
Fig. 4-50 Crack patterns of slot connection type

The crack patterns of the superstructure with PHC connection type are shown in

Fig. 4-51. PHC connection type showed inefficient performance. However, in superstructure model, The performance of PHC connection type showed similar with the RO + TO model. The number of damaged elements (1074) were small compared to RO + TO model. The stiffness of PHC connection type was non-linear in previous study, however, the inserted stiffness data was changed linear, and the changed stiffness data was similar with the RO + TO model, therefore RO + TO model shows the inefficient performance.

(a) Crack patterns at the edge

(b) Crack patterns in mid-span
Fig. 4-51 Crack patterns of PHC connection type

Fig 4-52 shows the results of 80 mm slot connection. The performance of slot connection was increased compared to the 40 mm slot connection. Furthermore, the number of damaged elements decreased from 295 (40 mm slot connection) to 258 (80 mm slot connection), which indicated that an increased slot size could increase the performance of the superstructure and abutment.
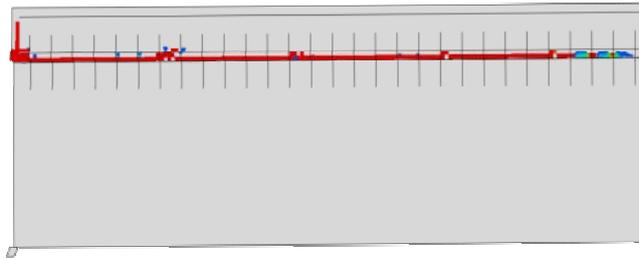
(a) Crack patterns at the edge
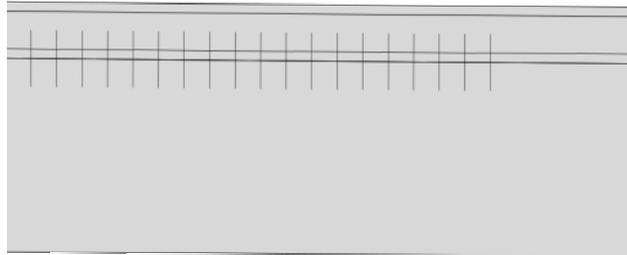
(b) Crack patterns in mid-span
Fig. 4-52 Crack patterns of 80 mm slot connection type

The damaged elements of the concrete are shown in Table 7, the results of the superstructure models are shown in Fig. 4-53. In increased stiffness models, the spiral rebar was efficient compared to other increased stiffness models. The flexible connection types showed better performance compared to increased stiffness connection types, however, when connection type is used, the axis-force due to superstructure should be considered.
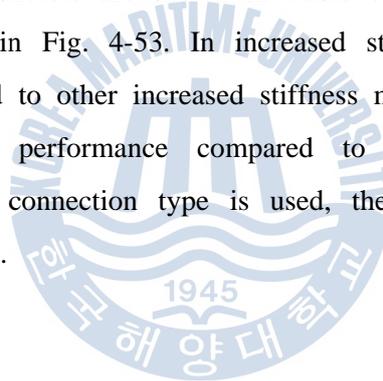
Table 7 Damaged elements of pile-to-pilecap connection

Connection type	The number of damaged elements
RO + TO	1205
PennDOT	1187
Square rebar	999
Grid rebar	932
HSS tube	1216
Spiral rebar	863
Removed flange	882
Reduced flange	827
Reduced flange with spiral rebar	827
Hole type	1074
Extended hole	511
Slot connection	295
PHC	1212
80 mm slot	258

Fig. 4-53 The number of damaged elements of superstructure models

Chapter 5

Conclusions and Recommendations

In this study, new pile-to-pilecap connections were developed and developed connections were evaluated. The parametric studies of developed pile-to-pilecap connections were conducted and evaluated. It was found that the developed connections can resist 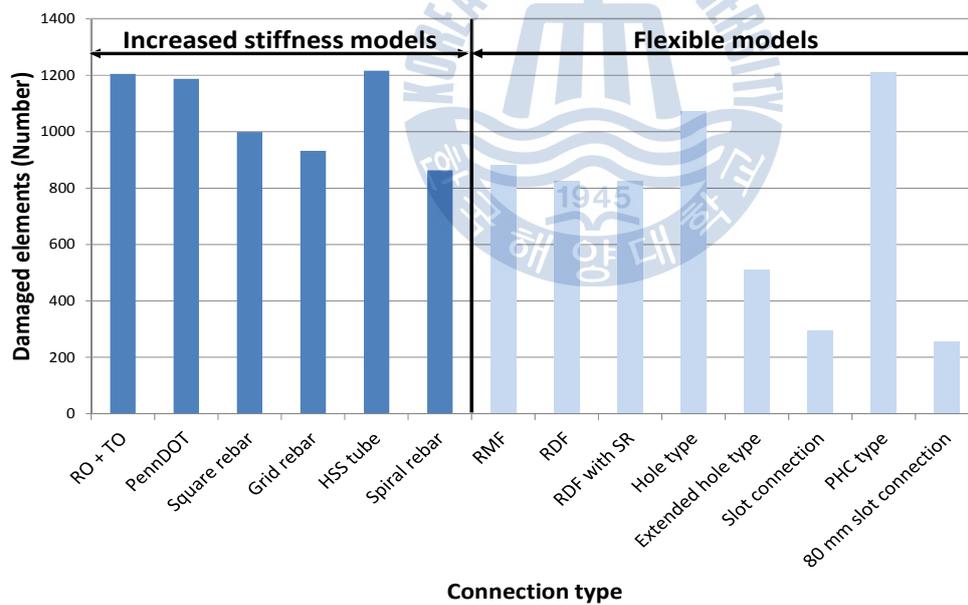up to 100 mm thermal displacement of superstructures. Followings are the conclusions derived from obtained results of this study.

5.1 Conclusions from Proposed Connections

- The developed models using Abaqus explicit 6.13 with the concrete damage plasticity model well predicted the experimental behavior of pile-to-pilecap connection.

- The performance of the IA bridges against thermal movement improved by flexible connections that allowed larger displacements and lower reactions.

- To increase the stiffness and mitigate possible four-way diagonal cracks from the HP pile, using rebar (PennDOT, Square rebar, Grid rebar) did not effectively improve the connection performance.

- The HSS tube connection type reduce the crack propagation. However, the second crack was occurred, results in earlier failure and small energy absorption compared to RO + TO model.

- The HSS tube connection type, hole connection type and PHC connection type were not recommended because it caused earlier complete crack failure.

- As flanges were removed, the reaction forces were reduced approximately up to 25% compared to the reaction forces of spiral rebar connection type.

- Extended hole and slot connections allowed 20 mm displacements without reaction forces.

- The behavior of the PHC connection type was brittle failure. Therefore, PHC connection types are not recommended for the pile-to-pilecap connection.

- The energies of extended hole and slot connection generated against a 100 mm displacement were smaller than spiral rebar connections. This indicates that the proposed connections of this study performed better in terms of minimized reaction forces and crack prevention.

5.2 Conclusions from Parametric Study

- In the parametric study of spiral rebar, a smaller pitch spacing increased resistant capacity of the pilecap. Therefore, the pitch spacing should be considered in design code.

- In the parametric study of spiral rebar, a larger rebar diameter showed more efficient performance compared to a smaller diameter. Therefore, the diameter of spiral rebar should be considered in design code.

- The results of parametric study of spiral rebar, a narrow width increased the reaction forces. Therefore, the width of spiral rebar should be considered in design code.

- In the asymmetry spiral rebar, a top rebar width in pilecap did not influence the performance of the pile-to-pile connection. Therefore, bottom rebar width should be considered in design code.

- In the parametric study on square rebar, the stiffness was increased linearly according to the number of rebar. Therefore, quantity of rebar should be considered in design code.

5.3 Conclusions from Superstructure Model

· In Slot connection type, the crack of superstructure did not propagate due to allowed displacement.

· Increased rotational stiffness showed a decrease in crack to the superstructure.

· In slot connection type, an increased slot length showed better performance of the superstructure.

· Increased stiffness of pile-to-pilecap connection did not influence the performance of the superstructure, whereas the flexible models were increased the performance of the superstructure.

· The slot connection is the best choice to improve the performance of a bridge because of effective behavior.

5.4 Recommendations for Further Study

· To predict more accurately data, soil-pile interaction, backfill-pile interaction and gravity load should be considered in analysis.

· The soft ground condition should be considered.

· To ensure analysis data, experiment should be conducted. Furthermore, analysis data should be compared to experimental data.

· In PHC connection type, fixed bottom surface of pile was damaged before flexible behavior of the pile-to-pilecap connection. Therefore, the PHC connection type should be improved and analysis should be conducted.

· The thermal load is changed daily. Therefore, the analysis for cyclic load should be considered to observe the detail behavior.

· The optimization study of the slot connection should be conducted.

· The analysis of fatigue for pile-to-pilecap connection will be conducted.

・ 3D superstructure model should be developed and conducted to observe the detail crack patterns of the superstructure.

Acknowledgement

Bibliography

ABAQUS, 2013, ABAQUS Documentation, Dassault Systèmes, Providence, RI, U.S.A.

Arockiasamy M., Butrieng N. & Sivakumar M.,2004, State-of-the-Art of Integral Abutment Bridges: Design and Practice, *Journal of Bridge Engineering*, ASCE, vol. 9, No. 5, pp. 497-506

Arsoy, S., Duncan, J. M. , & Barker, R. M., 2002, Performance of Supporting integral Bridges, Transportation Research Record, *Journal of the Transportation Research Board*, No.1808, Transportation Research Board of the National Academies, Washington D.C., pp. 162-167

Ahn, J.H., Yoon, J.H., Kim, J.H. & Kim, S.H., 2011, Evaluation on the behavior of abutment-pile connection in integral abutment bridge. *Journal of Constructional Steel Research*, vol 67, pp. 1134-1148

Baptiste K., Kim W. & Laman J. A., 2011, "Parametric Study and Length Limitations for Prestressed Concrete Girder Integral Abutment Bridges", *Journal of the International Association for Bridge and Structural Engineering (LABSE)*, Vol. 21, No. 2, pp.151-156

Dicleli, M. & Albhaisi, S. M., 2004, Effect of cyclic thermal loading on the performance of steel H-piles in integral bridges with stub-abutments, Journal of Constructional Steel Research, Vol 60, pp. 161-182

Frosch, R. J., Kreger, M. E. & Talbott, A. M., 2009, *Earthquake Resistance of integral Abutment Bridges*, FHWA / IN /JTRP - 2008/11, Joint Transportation Research Program, Indiana Department of Transportation and Purdue University

International Federation for Structural Concrete, 2010, *CEB-FIP MODEL CODE 2010*, Lausanne Switzerland

Kalayci E., Civjan S. A. & Brena S. F., 2012, Parametric study on the thermal response of curved integral abutment bridges, *Journal of Engineering Structures*, Vol 43, pp. 129-138

Kim, W.S. & Laman, J. A., 2010a, Integral Abutment Bridge Response under Thermal

Loading, *Engineering structures*, Vol. 32, No. 6, pp. 1495-1508.

Kim, W.S. & Laman, J. A., 2010b, Numerical Analysis Method for Long-term Behavior of integral Abutment Bridges, *Engineering Structures*, Vol. 32, No.8, pp. 2247-2257

Kim, W.S. & Laman, J. A., 2012, Seven-year Field Monitoring of Four integral Abutment Bridges, *Journal of Performance of Constructed Facilities*, Vol. 26, No. 1, pp. 54-64

Kim, W.S., Lee, J.H. & Jeoung, C., 2013a, Concrete Crack Control of Pile-to-pilecap Connection in integral Abutment Bridges under Cyclic Bridge Movement. *3rd International Conference on Adbanced Engineering Materials and Technology*, Zhangjiajie, China

Kim, W.S., Lee, J.H. & Cho, D.Y., 2013b, Crack Analysis of Pile-abutment Connection in Concrete Integral Abutment Bridges, *Korea Concrete Institute Spring 2013 Convention*, Yeosu, May 14-16, Korea Concrete Institute, pp. 559-560

Kim, W.S., Lee, J.H. & Park T.H., 2013c, Development of Abutment-H pile Connection for Large Lateral Displacements of Integral Abutment Bridges, *Computational Structural Engineering Institute of Korea*, Vol. 26, No. 4, pp.309~318

Minister of Construction and Transportation. 2012, *Korean Highway Bridge Design Code 2012*

Kunin J., & Alampalli S., 2000, Integral Abutment Bridges : Current Practice in United States and Canada, *Journal of Performance of Constructed Facilities*, Vol. 14, No. 3, pp. 101-111

Lee, J.H., Kim W.S. & Kim K.J., 2014, A parametric Study of The Pile-to-pilecap Connection Reinforced with Spiral Rebar, *Korea Institute for Structural Maintenance and Inspection Spring 2014 Conference*, Daegu, April 10-12, Korea Institute for Structural Maintenance and Inspection, Vol. 18, No. 1, pp. 614-615

Lee, J.H, Kim, W.S. & Kim K.J., 2014, Structural Evaluation of Proposed Connections in Integral Abutment Bridges, *Korea Institute for Structural Maintenance and Inspection Spring 2014 Conference,* Daegu*,* April 10-12, Korea Institute for Structural Maintenance and Inspection, Vol. 18, No. 1, pp. 616-618

Lee, J. & F. L. Fenves, 1998, Plastic-Damage Model for Cyclic Loading of Concrete

Structures, *Journal of Engineering Mechanics*, vol. 124, no.8, pp.892-900

Lubliner, J., J. Oliver, S. Oller, & E. Onate, 1989, A Plastic-Damaged Model for Concrete, *International Journal of Solids and Structures*, Vol. 25, pp. 299-329

Pennsylvania Department of Transportation (PennDOT), 2007, *Design Manual Part 4, Structures: Procedures-Design-Plans Presentation*, PennDOT Design 252 Manual Part 4, Commonwealth of Pennsylvania, Department of Transportation, Harrisburg, PA